Extravascular spaces are the primary reservoir of antigenic diversity in *Trypanosoma brucei* infection

Authors: Alexander K. Beaver[1,2], Zhibek Keneskhanova[3,4], Raúl O. Cosentino[3,4], Brian L. Weiss[5], Erick O. Awuoche[5], Gretchen M. Smallenberger[5], Gracyn Y. Buenconsejo[2], Nathan P. Crilly[1,2], Jaclyn E. Smith[2], Jill M.C. Hakim[2], Bailin Zhang[2], Bryce Bobb[2], Filipa Rijo-Ferreira[6,7,8], Luisa M. Figueiredo[6], Serap Aksoy[5], T. Nicolai Siegel[3,4], and Monica R. Mugnier[2]†.

Affiliations:

[1]Department of Pathology, Johns Hopkins School of Medicine; Baltimore, Maryland, United States of America

[2]Department of Molecular Microbiology and Immunology, Johns Hopkins Bloomberg School of Public Health; Baltimore, Maryland, United States of America

[3]Division of Experimental Parasitology, Faculty of Veterinary Medicine, Ludwig-Maximilians-Universität München, Munich, Germany

[4]Biomedical Center, Division of Physiological Chemistry, Faculty of Medicine, Ludwig-Maximilians-Universität München, Munich, Germany

[5]Department of Epidemiology of Microbial Diseases, Yale School of Public Health; New Haven, Connecticut, United States of America

[6]Instituto de Medicina Molecular, Faculdade de Medicina, Universidade de Lisboa, Lisboa, Portugal

[7]Department of Neuroscience, Peter O'Donnell Jr. Brain Institute, University of Texas Southwestern Medical Center; Dallas, Texas, United States of America

[8]Division of Infectious Diseases and Vaccinology, Berkeley Public Health Molecular and Cell Biology Department; Berkeley, California, United States of America

† Corresponding author. Email: mmugnie1@jhu.edu

Summary paragraph: The protozoan parasite *Trypanosoma brucei* evades clearance by the host immune system through antigenic variation of its dense variant surface glycoprotein (VSG) coat, periodically "switching" expression of the VSG using a large genomic repertoire of VSG-encoding genes[1–6]. Recent studies of antigenic variation in vivo have focused near exclusively on parasites in the bloodstream[4,7,8], but research has shown that many, if not most, parasites reside in the interstitial spaces of tissues[9–13]. We sought to explore the dynamics of antigenic variation in extravascular parasite populations using VSG-seq[7], a high-throughput sequencing approach for profiling VSGs expressed in populations of *T. brucei*. Here we show that tissues, not the blood, are the primary reservoir of antigenic diversity during both needle- and tsetse bite-initiated *T. brucei* infections, with more than 75% of VSGs found exclusively within extravascular spaces. We found that this increased diversity is correlated with slower parasite clearance in tissue spaces. Together, these data support a model in which the slower immune response in extravascular spaces provides more time to generate the antigenic diversity needed to maintain a chronic infection. Our findings reveal the important role that extravascular spaces can play in pathogen diversification.

Main: Every pathogen must contend with the adaptive immune response of its host. *Trypanosoma brucei,* a protozoan parasite and causative agent of human and animal African Trypanosomiasis, has evolved a sophisticated strategy to evade this highly flexible and specific host response[14]. Transmitted by the bite of the tsetse fly, *T. brucei* lives extracellularly in the blood, lymph, and interstitial tissue spaces of its mammalian host[15]. To escape clearance by a continuous onslaught of host antibodies, the parasite periodically "switches" expression of its immunogenic variant surface glycoprotein (VSG) coat to new, antigenically distinct variants[1]. With a genomic repertoire of thousands of different VSG-encoding genes[2,3,5,6] and the ability to generate novel VSGs through recombination[4,8,16], the parasite has an enormous capacity for altering its antigenic profile.

Studies examining *T. brucei* antigenic variation in vivo have focused nearly exclusively on parasites in the blood, revealing complex VSG expression dynamics[4,7,8]. However, it has recently become clear that many, if not most, *T. brucei* parasites inhabit extravascular spaces during both experimental and natural infections[9–13]. Though research has shown that tissue-resident parasites adapt to these environments[11], cause tissue-specific symptoms[15], and are associated with increased disease severity[13], it remains unclear why parasites invade tissue spaces and what role these populations might play in infection.

Several older studies suggested a role for tissue-resident parasites in antigenic variation. These studies found that brain- and lymph-resident parasite populations were antigenically distinct from those in the blood[17–20], and that antigenic types detectable in the lymphatic fluid could be detected in the blood at later timepoints during infection[19]. This led these researchers to hypothesize that extravascular spaces might be a site for antigenic variation, with antigenic variants generated in extravascular spaces contributing to systemic immune evasion. However, a later study focusing on very early timepoints post-infection found no antigenic difference between *T. brucei* populations within the blood and several extravascular spaces[21], and the community consequently ruled out a role for extravascular parasites in antigenic variation[22,23]. These early investigations were limited by the methodology available at the time, which relied on the use of VSG-specific antisera to analyze parasite antigenic diversity. Modern high-throughput sequencing methods allow VSG expression to be measured accurately and in high resolution[7]. Given the mounting evidence that *T. brucei* parasites persist in and adapt to extravascular spaces, there is a clear need to reinvestigate the dynamics of VSG expression within tissue spaces.

Here, we use VSG-seq[7], a targeted RNA-sequencing approach for profiling the VSGs expressed in *T. brucei* populations, to characterize the VSGs expressed by extravascular *T. brucei* parasites. Our results show that extravascular spaces are major reservoirs of antigenic diversity during *T. brucei* infection and that this parasite niche is central to the parasite's ability to continuously outmaneuver the immune system.

Extravascular spaces contain most of the VSG diversity

To investigate how tissue-resident parasites contribute to antigenic variation in vivo, we intravenously (IV) infected 12 mice, each with ~5 pleomorphic *T. brucei* EATRO1125 90-13 parasites[24]. We collected blood, then perfused mice with PBS-glucose (Extended Data Fig. 1) and harvested the heart, lungs, gonadal fat, subcutaneous fat, brain, and skin at 6, 10, and 14 days post-infection. For each sample, we extracted RNA and quantified *T. brucei* VSG expression using VSG-seq[7]. A single "initiating" VSG (either AnTat1.1 or EATRO1125 VSG-421)

dominated expression in both the blood and tissues on day 6 (Fig. 1a), in line with previous observations[21,25]. At later time points, VSG expression dynamics became more complex, with more VSGs expressed, a unique composition of VSGs in each tissue, and no single dominating variant (Fig. 1a). Although tissue-specific expression of variant surface proteins is a feature in other organisms that use antigenic variation[26–31], we found no evidence for tissue-specific VSGs or VSG sequence motifs (Extended Data Fig. 2). Instead, we observed an increase in antigenic diversity in extravascular spaces. The number of detectable VSGs in tissue spaces was, on average, two to four times higher than the blood (Fig. 1c). This did not correlate with parasite load (Extended Data Fig. 3 and Extended Data Fig. 4ab) and was not driven by any specific tissue (Fig. 1d). In addition, parasite differentiation to the non-dividing tsetse infective form via quorum sensing, which is marked by expression of the PAD1 gene[32], did not correlate with VSG diversity in either the blood or tissues at the population level (Extended Data Fig. 4c). The overall contribution of tissue-resident parasites to antigenic diversity in a single infection was large: at any time, ~87% of expressed VSGs in any individual infection were found exclusively within extravascular spaces (Fig. 1b).

VSG-seq is a bulk measure of VSG expression. To be sure that the increased VSG diversity we observed in tissues was not due to the derepression of silent VSGs within individual cells, we performed single-cell RNA sequencing using the SL-Smart-seq3xpress platform to quantify VSG expression in single cells from blood and tissue samples[33]. Because *T. brucei* can form new "mosaic" VSGs through recombination[4,8,16,34], which are, by definition, absent from reference genomes, we initially used our VSG-Seq pipeline to *de novo* assemble VSGs in each cell. This approach accounts for the possibility that expressed VSGs might be absent from the reference genome, either as a result of mosaic VSG formation or as a result of an incomplete genome assembly, potentially affecting quantification and/or read mapping. Only one VSG assembled in most cells (94.2%; Extended Data Fig. 5a). We also mapped sequencing reads to the EATRO1125 genome, which could reveal more subtle signatures of derepression. By this analysis, there was no obvious difference between the blood and the tissues in the number of expressed VSGs in each cell (Extended Data Fig. 5b) or in the relative expression of the most abundant VSG in each cell (Extended Data Fig. 5c).

To estimate the number of cells maintaining monogenic expression, we defined a cell as maintaining monogenic expression if 80% of UMIs mapping to VSGs mapped to a single VSG. Although mapping to the genome suggested that most cells (62.7%) maintained monogenic expression based on this threshold, the proportion of cells estimated to maintain monogenic expression was lower than estimated by *de novo* assembly. Comparison of the two analyses revealed that of those cells expressing >1 VSG by genome alignment, 85% were found to express only one VSG by mapping to the *de novo* assembled VSGs and using the same 80% threshold for defining monogenic expression. Further investigation revealed that in most of these cases (95.3%) the alignment to multiple genomic VSGs was an artifact, where the assembled VSG was not well represented within the annotated sequences of the EATRO1125 genome or there were several VSGs with high similarity to the assembled VSG, leading to inaccurate VSG expression quantification (Extended Data Fig. 5d). We estimate that 93.4% of cells were likely expressing only one VSG, with no bias for multigenic VSG expression in tissue spaces (Extended Data Fig. 5e, shades of green and Extended Data Table 2). In 5.2% of cells, reads mapped to multiple EATRO1125 VSGs, but no VSG could be assembled (grey). While it is impossible to distinguish between multi- and monogenic VSG expression in this set of cells, the proportion of cells in this category did not differ between blood and tissues. The few cells that

131 appear to express multiple VSGs (1.05% of cells in the blood and 1.03% of cells in the tissues)
132 could indicate sorting doublets or, more interestingly, could represent cells mid-switch
133 (Extended Data Fig. 5e, red and purple). Overall, these data suggest that VSG monogenic
134 expression is maintained by most cells in both extravascular spaces and the blood and that the
135 increased VSG diversity we observe in tissue spaces is unlikely to be due to the specific
136 derepression of silent VSGs in tissue populations.

137 **Frequently expressed VSGs first appear in tissue populations**

138 The high antigenic diversity observed in tissues could serve to maintain a chronic infection. If
139 antigenic variation occurs relatively rarely in the bloodstream, then parasites from extravascular
140 spaces might serve as a source of new, antigenically distinct, VSGs. In line with this, tissue
141 spaces contain more "unique VSGs", those VSGs that are expressed exclusively within one
142 space in an infection, than the blood (Fig. 2ab). To examine the potential for tissue-resident
143 VSGs to contribute to antigenic variation systemically, we identified VSGs only expressed in
144 tissues on day 6 post-infection and analyzed whether they later appeared within the blood. The
145 majority (74%) of these VSGs were expressed within the blood on day 10 or 14. Analysis of
146 individual VSGs revealed that rare VSGs expressed at low levels exclusively in tissue spaces
147 also have the potential to become ubiquitously expressed within a host (Fig. 2c). In addition to a
148 model in which tissue spaces provide new VSGs to re-seed the blood, it is possible that tissue-
149 resident parasites undergo antigenic variation before blood-resident populations. Therefore, these
150 data could be explained by either a trigger within the tissue environment that induces parasite
151 switching or a differential selective pressure imposed by the tissue environment.

152 **VSG-specific parasite clearance is delayed in tissues compared to the blood**

153 Indeed, our data suggest that the environment within tissue spaces is distinct from the blood,
154 with parasite clearance occurring at different rates in each space. While parasites expressing the
155 initiating VSG were cleared from the blood by day 10 post-infection, they were not cleared from
156 tissues until at least day 14 (Fig. 3a). This suggests that VSG-specific parasite clearance from
157 extravascular spaces is delayed, but not abolished, compared to the blood. VSG-seq is a measure
158 of VSG expression at the transcript level, however. To confirm this observation at the protein
159 level, we performed flow cytometry on *T. brucei* cells from the blood, lungs, and gonadal fat,
160 using the tdTomato-expressing "triple reporter" *T. brucei* EATRO1125 AnTat1.1E cell line[35]
161 (Fig. 3bc). The flow cytometry analysis showed a detectable AnTat1.1-expressing tissue parasite
162 population at day 13 post-infection, a timepoint at which AnTat1.1^{+} parasites were undetectable,
163 or nearly undetectable, in the blood. Similar to the increase in antigenic diversity we observed in
164 every tissue space, this delay in clearance, observed at both the RNA and protein levels, was not
165 tissue-specific. Thus, the immune mechanisms influencing extravascular parasite clearance
166 appear to be general features of extravascular spaces.

167 **Infections initiated by tsetse fly bite also show increased diversity and delayed clearance in**
168 **extravascular spaces**

169 A benefit of starting infections with a small intravenous inoculum is that it creates convenient
170 and reproducible infections. In nature, however, a tsetse fly bite introduces thousands of parasites
171 into the skin, each expressing a single metacyclic VSG (mVSG) from a limited repertoire[36]. To
172 ensure that our observations held true in this more complex context, we repeated our infections
173 using a more natural tsetse bite infection model. Infections were initiated in 5 mice by tsetse bite
174 using flies infected with RUMP 503 *T. brucei* parasites[37]. We used VSG-seq to quantify VSG

expression in the blood on day 5 post-infection and the blood and tissues on day 14 post-infection. In line with our previous observations, we found that in tsetse-initiated infections ~80% of VSGs were exclusively expressed within extravascular spaces (Fig. 4a) and tissue populations harbored more VSGs than the blood (Fig. 4b). This demonstrates that extravascular spaces are the primary reservoir of antigenic diversity, even when infections are initiated by fly bite.

Parasite populations were more diverse at early time points in tsetse infections than IV infections, likely due to the larger and more heterogeneous inoculum delivered by the fly. To analyze VSG-specific parasite clearance in tissues, we quantified expression of the most abundantly expressed VSG in the blood of each mouse on day 5 as well as the known mVSG repertoire from this parasite strain, which should represent the repertoire of VSGs expressed at the start of an infection. In both cases, we found that on day 14, tissue spaces still contained parasites expressing the most abundant VSG and/or mVSGs, while these VSGs were expressed by no or very few parasites in the blood (Fig. 4c,d). This suggests that in tsetse-bite-initiated infections, as we observed in IV infections, tissue parasite populations are cleared at a slower rate than parasites in the blood.

Delayed clearance of parasites leads to increased VSG diversity

The increased antigenic diversity in extravascular spaces could be explained by the distinct clearance dynamics we observe, as prolonged survival in tissues could provide more time for parasites to switch. To test whether there was a link between parasite survival and increased diversity, we sought to interrupt parasite clearance in tissues. Because parasite clearance in the blood coincides with the appearance of anti-VSG IgM, between days 8 and 10, and parasite clearance in the tissues coincides with the anti-VSG IgG response, between days 10 and 14[1,12,38–41], we hypothesized that clearance in tissues is dependent on the anti-VSG IgG response. Thus, the loss of IgG might abrogate the clearance of tissue-resident parasites. To test this hypothesis, we infected activation-induced cytidine deaminase (AID) knockout (AID Cre) mice[42], which only produce IgM antibodies (Extended Data Fig. 6), and analyzed blood and tissues from days 6 and 14 post-infection by VSG-seq. As expected, clearance of the initiating VSG was severely delayed in tissues on day 14 in $AID^{-/-}$ mice, suggesting that IgG is important, if not critical, for the clearance of extravascular parasites. This could be explained by the fact that IgM, a bulky pentamer, does not diffuse efficiently into tissue spaces[43,44], while IgG, a monomer, readily diffuses. We also observed a defect in the clearance of blood-resident parasites in $AID^{-/-}$ mice compared to the blood of WT mice (Fig. 5a). In both the blood and tissues of $AID^{-/-}$ mice, where clearance was delayed, more VSGs were detected on day 14 post-infection compared to wild-type (Fig. 5b), revealing a direct relationship between the timing of parasite clearance and VSG diversity. Regardless of their local environment (intra- or extravascular), longer-lived parasite populations generated more diverse sets of VSGs.

Discussion

The idea that antigenic variation might occur outside of the bloodstream, with extravascular populations contributing to immune evasion within the bloodstream, is not a new one. Here, using modern high-resolution techniques, we provide evidence for this long-standing hypothesis. In both needle- and tsetse bite-initiated infections, we find that extravascular spaces are the primary reservoir of VSGs, accounting for the vast majority of antigenic diversity in any individual infection. The number of VSGs we detected in the blood matches previous

219 estimates[4,7,8], while the diversity in tissues is two to four times higher. Our data suggest that this
220 is at least partially due to slower clearance dynamics in extravascular spaces and highlight the
221 role that tissue spaces can play in pathogen diversification.

222 Although extravascular parasite populations were highly antigenically diverse, we saw no
223 evidence of tissue-specific VSG expression. Because parasites invade tissues efficiently before
224 much VSG switching has occurred, it appears unlikely that any specific VSG is required for
225 tissue invasion. Whether VSGs could influence parasite fitness in specific host spaces is less
226 clear. We measured VSG expression up to day 14 post-infection, at which point tissue-resident
227 populations are just beginning to diverge from one another and the blood. It is therefore possible
228 that, as these populations further evolve, there may be a selection for VSGs better adapted to
229 certain tissue spaces.

230 It has previously been shown that in the bloodstream alone *T. brucei* expresses more VSGs than
231 appear to be required for immune evasion[7]. Here we find that the expressed VSG diversity within
232 host tissues is even greater. While on the surface it could appear to be disadvantageous for *T.*
233 *brucei* to use so many different antigens this quickly, this striking diversity could be important
234 for the parasite. In natural infections, particularly in wild animals where pre-existing anti-VSG
235 immunity is more likely to exist, a high switch rate may be required to ensure some parasites
236 successfully evade the host's existing antibody repertoire. Moreover, infections in the wild can
237 last for months to years[14,45]. During these long infections, the large reservoirs of VSGs found in
238 tissues may be essential for the maintenance of a chronic infection.

239 Indeed, our data support the idea that the large reservoirs of antigenic diversity in extravascular
240 spaces contribute to systemic infection when parasites re-enter the blood after switching: rare
241 VSGs expressed exclusively in tissues at early time points are expressed in the blood and other
242 spaces later. This is also in line with another recent study which showed that blood-resident
243 parasites are largely non-replicative, indicating that tissue-resident parasites may be required to
244 re-seed the blood[46]. There is another intriguing explanation for this observation, however.
245 Switching in *T. brucei* is known to be semi-predictable[7,47], and it is possible that tissue-resident
246 parasites simply switch earlier, or more frequently, than those in the blood. In this case, the same
247 VSGs would arise independently in every population without any parasite movement between
248 spaces. While the high vascular permeability observed after the initial stages of infection
249 indicates that parasites likely move back and forth between the vasculature and extravascular
250 spaces, the fact that tissue-resident populations contain many unique VSGs suggests that blood
251 re-entry may represent a bottleneck for the parasite. An increased rate of switching in tissues
252 could be explained by a higher proportion of dividing slender form parasites in these spaces, as
253 has been observed in the adipose tissue[13], but we found no correlation at the population level
254 between PAD1 expression and increased VSG diversity. Notably, increased diversity is still
255 observed when the overall parasite load in tissues is lower than the blood (Extended Data Fig
256 3c). It is therefore exciting to speculate that some aspect of the extravascular environment
257 supplies a molecular or physical stimulus that promotes VSG switching.

258 While the timing of VSG switching could be the result of an environmental trigger, our data
259 suggest that the higher antigenic diversity in extravascular spaces compared to the blood can also
260 be explained, at least in part, by the dynamics of the immune response to *T. brucei* in each space.
261 In tissue spaces, we observed slower VSG-specific clearance of parasites than in the blood,
262 potentially providing these populations more time to undergo antigenic variation. Additionally,
263 newly switched parasites are still vulnerable to immune clearance by antibodies against their

264 previous VSG for ~29 hours, so moderate delays in immune clearance could allow more
265 switched parasites to survive[48]. The direct relationship we observed between the timing of
266 parasite clearance and antigenic diversity in AID$^{-/-}$ mice supports this model, with even small
267 delays in clearance showing major effects on parasite VSG diversity in both the tissues and the
268 blood.

269 Our results show that the production of IgG plays a key role in clearing parasites from tissues,
270 which we propose could be related to the ready diffusion of this molecule within extravascular
271 spaces facilitating parasite clearance. It is important to note, however, that while the difference in
272 timing between the anti-VSG IgM and IgG responses inspired the hypothesis that IgG might be
273 important for parasite clearance in tissues, our study does not prove that this difference in timing
274 explains the delayed clearance in tissue spaces. The local immune response to *T. brucei* is
275 complex, with multiple mechanisms likely to play a role in parasite detection and clearance; our
276 results suggest that IgG is an important player in this response. The increased VSG diversity we
277 observe is certainly multifactorial and could be influenced by parasite factors, such as
278 metabolism, division, motility, and antibody internalization, and host factors, such as
279 extravascular environmental stresses, the local immune response, and vascular permeability.
280 More research will be required to fully understand the complex nature of the *T. brucei* host-
281 pathogen interaction within the extravascular niche.

282 Altogether, our results outline a model in which *T. brucei* parasites "hide" in extravascular
283 spaces to generate new antigenic variants capable of exiting tissues and aiding in systemic
284 immune evasion. Coupled with other recent studies[9–13,46,49], this suggests a framework for the
285 progression and pathogenesis of *T. brucei* infections where, instead of being the primary parasite
286 reservoir, the blood may represent a transient population that is regularly re-seeded by
287 extravascular parasites. The vasculature, then, might act as a highway system for movement
288 between the tissue spaces and for eventual transmission back into the tsetse fly.

289 Interfering with the egress from or establishment within tissue spaces might be a strategy for
290 treating *T. brucei* infections or other infections with pathogens that rely on the distinct features of
291 the extravascular environment. In line with this, one recent study showed that partial inhibition
292 of *T. brucei* tissue invasion using antibodies against P- and E-selectins results in prolonged
293 survival in mice[13]. This also fits with data from another group that found immotile *T. brucei*
294 parasites, likely unable to invade tissues, were no longer infectious[50]. It is possible that without
295 the proper establishment of parasite tissue reservoirs, overall antigenic diversity is lowered,
296 limiting the parasite's capacity for immune evasion and leading to a decrease in parasite burden.
297 Defining the dynamics and variation of parasites both within and between spaces, as well as the
298 unique host environment within each tissue space, will be central to understanding how *T. brucei*
299 consistently avoids immune clearance and harnessing this mechanism for disease control.

300 More broadly, these data demonstrate how different environmental and immune pressures within
301 a host can influence pathogen diversification. This production of genetic heterogeneity within an
302 infection is important for many pathogen virulence processes, including establishing and
303 maintaining infection, facilitating immune evasion, generating drug resistance, and adapting to
304 different host environments. The extravascular environment plays a unique role in promoting
305 pathogen evolution, and *T. brucei* serves as a valuable model for understanding this aspect of the
306 host-pathogen interface.

307

308 **References:**

309 1. Magez, S. *et al.* The Role of B-cells and IgM Antibodies in Parasitemia, Anemia, and
310 VSG Switching in Trypanosoma brucei–Infected Mice. *PLoS Pathog.* **4**, e1000122 (2008).

311 2. Cross, G. A. M., Kim, H. S. & Wickstead, B. Capturing the variant surface glycoprotein
312 repertoire (the VSGnome) of Trypanosoma brucei Lister 427. *Mol. Biochem. Parasitol.*
313 **195**, 59–73 (2014).

314 3. Müller, L. S. M. *et al.* Genome organization and DNA accessibility control antigenic
315 variation in trypanosomes. *Nat. 2018 5637729* **563**, 121–125 (2018).

316 4. Hall, J. P. J., Wang, H. & David Barry, J. Mosaic VSGs and the Scale of Trypanosoma
317 brucei Antigenic Variation. *PLoS Pathog.* **9**, (2013).

318 5. Hertz-Fowler, C. *et al.* Telomeric Expression Sites Are Highly Conserved in
319 Trypanosoma brucei. *PLoS One* **3**, e3527 (2008).

320 6. Cosentino, R. O., Brink, B. G. & Nicolai Siegel, T. Allele-specific assembly of a
321 eukaryotic genome corrects apparent frameshifts and reveals a lack of nonsense-mediated
322 mRNA decay. *NAR Genomics Bioinforma.* **3**, (2021).

323 7. Mugnier, M. R., Cross, G. A. M. & Papavasiliou, F. N. The in vivo dynamics of antigenic
324 variation in Trypanosoma brucei. *Science* **347**, 1470–3 (2015).

325 8. Jayaraman, S. *et al.* Application of long read sequencing to determine expressed antigen
326 diversity in Trypanosoma brucei infections. *PLoS Negl. Trop. Dis.* **13**, e0007262 (2019).

327 9. Capewell, P. *et al.* The skin is a significant but overlooked anatomical reservoir for
328 vector-borne African trypanosomes. *Elife* **5**, (2016).

329 10. Camara, M. *et al.* Extravascular Dermal Trypanosomes in Suspected and Confirmed Cases
330 of gambiense Human African Trypanosomiasis. *Clin. Infect. Dis. An Off. Publ. Infect. Dis.*
331 *Soc. Am.* **73**, 12 (2021).

332 11. Trindade, S. *et al.* Trypanosoma brucei Parasites Occupy and Functionally Adapt to the
333 Adipose Tissue in Mice. *Cell Host Microbe* (2016). doi:10.1016/j.chom.2016.05.002

334 12. Carvalho, T. *et al.* Trypanosoma brucei triggers a marked immune response in male
335 reproductive organs. *PLoS Negl. Trop. Dis.* (2018). doi:10.1371/journal.pntd.0006690

336 13. De Niz, M. *et al.* Organotypic endothelial adhesion molecules are key for Trypanosoma
337 brucei tropism and virulence. *Cell Rep.* **36**, 109741 (2021).

338 14. WHO. Control and surveillance of human African trypanosomiasis: Report of a WHO
339 Expert Committee. *WHO Tech. Rep. Ser.* 1–237 (2013).

340 15. Crilly, N. P. & Mugnier, M. R. Thinking outside the blood: Perspectives on tissue-resident
341 Trypanosoma brucei. *PLOS Pathog.* **17**, e1009866 (2021).

342 16. Kamper, S. M. & Barbet, A. F. Surface epitope variation via mosaic gene formation is
343 potential key to long-term survival of Trypanosoma brucei. *Mol. Biochem. Parasitol.* **53**,
344 33–44 (1992).

345 17. Seed, J. R. & Eefron, H. G. Simultaneous presence of different antigenic populations of
346 Trypanosoma brucei gambiense in Microtus montanus. *Parasitology* **66**, 269–278 (1973).

347 18. SEED, J. R., EDWARDS, R. & SECHELSKI, J. The ecology of antigenic variation. *J.*
348 *Protozool.* **31**, 48–53 (1984).

349 19. Barry, J. D. & Emery, D. L. Parasite development and host responses during the
350 establishment of Trypanosoma brucei infection transmitted by tsetse fly. *Parasitology* **88 (**
351 **Pt 1)**, 67–84 (1984).

352 20. Tanner, M., Jenni, L., Hecker, H. & Brun, R. Characterization of Trypanosoma brucei
353 isolated from lymph nodes of rats. *Parasitology* **80**, 383–391 (1980).

354 21. Turner, C. M., Hunter, C. A., Barry, J. D. & Vickerman, K. Similarity in variable antigen
355 type composition of Trypanosoma brucei rhodesiense populations in different sites within
356 the mouse host. *Trans. R. Soc. Trop. Med. Hyg.* **80**, 824–830 (1986).

357 22. Vickerman, K. Trypanosome sociology and antigenic variation. *Parasitology* **99 Suppl**,
358 S37–S47 (1989).

359 23. Barry, J. D. & Turner, C. M. R. The dynamics of antigenic variation and growth of
360 African trypanosomes. *Parasitol. Today* **7**, 207–211 (1991).

361 24. Engstler, M. & Boshart, M. Cold shock and regulation of surface protein trafficking
362 convey sensitization to inducers of stage differentiation in Trypanosoma brucei. *Genes*
363 *Dev.* **18**, 2798 (2004).

364 25. Turner, C. M. R. & Barry, J. D. High frequency of antigenic variation in Trypanosoma
365 brucei rhodesiense infections. *Parasitology* **99 Pt 1**, 67–75 (1989).

366 26. Salanti, A. *et al.* Evidence for the Involvement of VAR2CSA in Pregnancy-associated
367 Malaria. *J. Exp. Med.* **200**, 1197–1203 (2004).

368 27. Duffy, P. E. & Fried, M. Plasmodium falciparum adhesion in the placenta. *Curr. Opin.*
369 *Microbiol.* **6**, 371–376 (2003).

370 28. Jonsson, A. -B, Ilver, D., Falk, P., Pepose, J. & Normark, S. Sequence changes in the pilus
371 subunit lead to tropism variation of Neisseria gonorrhoeae to human tissue. *Mol.*
372 *Microbiol.* **13**, 403–416 (1994).

373 29. Nassif, X. *et al.* Antigenic variation of pilin regulates adhesion of Neisseria meningitidis
374 to human epithelial cells. *Mol. Microbiol.* **8**, 719–725 (1993).

375 30. Rudel, T., van Putten, J. P. M., Gibbs, C. P., Haas, R. & Meyer, T. F. Interaction of two
376 variable proteins (PilE and PilC) required for pilus-mediated adherence of Neisseria
377 gonorrhoeae to human epithelial cells. *Mol. Microbiol.* **6**, 3439–3450 (1992).

378 31. Virji, M. & Heckels, J. E. The role of common and type-specific pilus antigenic domains
379 in adhesion and virulence of gonococci for human epithelial cells. *J. Gen. Microbiol.* **130**,
380 1089–1095 (1984).

381 32. Dean, S., Marchetti, R., Kirk, K. & Matthews, K. R. A surface transporter family conveys
382 the trypanosome differentiation signal. *Nature* **459**, 213 (2009).

383 33. McWilliam, K. R. *et al.* High-resolution scRNA-seq reveals genomic determinants of
384 antigen expression hierarchy in African Trypanosomes. *bioRxiv* 2024.03.22.586247
385 (2024). doi:10.1101/2024.03.22.586247

386 34. Smith, J. E. *et al.* DNA damage drives antigen diversification through mosaic VSG

387 formation in Trypanosoma brucei. *bioRxiv* 2024.03.22.582209 (2024).
388 doi:10.1101/2024.03.22.582209

389 35. Calvo-Alvarez, E., Cren-Travaillé, C., Crouzols, A. & Rotureau, B. A new chimeric triple
390 reporter fusion protein as a tool for in vitro and in vivo multimodal imaging to monitor the
391 development of African trypanosomes and Leishmania parasites. *Infect. Genet. Evol.* **63**,
392 391–403 (2018).

393 36. Hutchinson, S. *et al.* The establishment of variant surface glycoprotein monoallelic
394 expression revealed by single-cell RNA-seq of Trypanosoma brucei in the tsetse fly
395 salivary glands. *PLOS Pathog.* **17**, e1009904 (2021).

396 37. Savage, A. F. *et al.* Transcript Expression Analysis of Putative Trypanosoma brucei GPI-
397 Anchored Surface Proteins during Development in the Tsetse and Mammalian Hosts.
398 *PLoS Negl. Trop. Dis.* **6**, 1708 (2012).

399 38. Schopf, L. R., Filutowicz, H., Bi, X. J. & Mansfield, J. M. Interleukin-4-Dependent
400 Immunoglobulin G1 Isotype Switch in the Presence of a Polarized Antigen-Specific Th1-
401 Cell Response to the Trypanosome Variant Surface Glycoprotein. *Infect. Immun.* **66**, 451
402 (1998).

403 39. Liu, G. *et al.* Distinct contributions of CD4+ and CD8+ T cells to pathogenesis of
404 trypanosoma brucei infection in the context of gamma interferon and interleukin-10.
405 *Infect. Immun.* **83**, 2785–2795 (2015).

406 40. Reinitz, D. M. & Mansfield, J. M. T-cell-independent and T-cell-dependent B-cell
407 responses to exposed variant surface glycoprotein epitopes in trypanosome-infected mice.
408 *Infect. Immun.* **58**, 2337–42 (1990).

409 41. Radwanska, M. *et al.* Comparative analysis of antibody responses against HSP60,
410 invariant surface glycoprotein 70, and variant surface glycoprotein reveals a complex
411 antigen-specific pattern of immunoglobulin isotype switching during infection by
412 Trypanosoma brucei. *Infect. Immun.* **68**, 848–860 (2000).

413 42. Robbiani, D. F. *et al.* Activation Induced Deaminase is required for the chromosomal
414 breaks in c-myc that lead to c-myc/IgH translocations. *Cell* **135**, 1028 (2008).

415 43. Hector, R. F., Collins, M. S. & Pennington, J. E. Treatment of Experimental Pseudomonas
416 aeruginosa Pneumonia with a Human IgM Monoclonal Antibody. *J. Infect. Dis.* **160**, 483–
417 489 (1989).

418 44. BARTH, W. F., WOCHNER, R. D., WALDMANN, T. A. & FAHEY, J. L. Metabolism
419 of Human Gamma Macroglobulins. *J. Clin. Invest.* **43**, 1036 (1964).

420 45. Mehlitz, D. & Molyneux, D. H. The elimination of Trypanosoma brucei gambiense?
421 Challenges of reservoir hosts and transmission cycles: Expect the unexpected. *Parasite*
422 *Epidemiol. Control* **6**, e00113 (2019).

423 46. Larcombe, S. D., Briggs, E. M., Savill, N., Szoor, B. & Matthews, K. The developmental
424 hierarchy and scarcity of replicative slender trypanosomes in blood challenges their role in
425 infection maintenance. *Proc. Natl. Acad. Sci. U. S. A.* **120**, e2306848120 (2023).

426 47. Morrison, L. J., Majiwa, P., Read, A. F. & Barry, J. D. Probabilistic order in antigenic
427 variation of Trypanosoma brucei. *Int. J. Parasitol.* **35**, 961–972 (2005).

428 48. Pinger, J., Chowdhury, S. & Papavasiliou, F. N. Variant surface glycoprotein density
429 defines an immune evasion threshold for African trypanosomes undergoing antigenic
430 variation. *Nat. Commun.* (2017). doi:10.1038/s41467-017-00959-w

431 49. Trindade, S. *et al.* Slow growing behavior in African trypanosomes during adipose tissue
432 colonization. *Nat. Commun. 2022 131* **13**, 1–13 (2022).

433 50. Shimogawa, M. M. *et al.* Parasite motility is critical for virulence of African
434 trypanosomes. *Sci. Rep.* (2018). doi:10.1038/s41598-018-27228-0

435 51. Fu, L., Niu, B., Zhu, Z., Wu, S. & Li, W. CD-HIT: accelerated for clustering the next-
436 generation sequencing data. *Bioinformatics* **28**, 3150 (2012).

437 52. So, J. *et al.* VSGs Expressed during Natural T. b. gambiense Infection Exhibit Extensive
438 Sequence Divergence and a Subspecies-Specific Bias towards Type B N-Terminal
439 Domains. *MBio* **13**, (2022).

440 53. Lee, J.-Y. & Kitaoka, M. A beginner's guide to rigor and reproducibility in fluorescence
441 imaging experiments. *https://doi.org/10.1091/mbc.E17-05-0276* **29**, 1519–1525 (2018).

442 54. Wirtz, E., Leal, S., Ochatt, C. & Cross, G. A. M. A tightly regulated inducible expression
443 system for conditional gene knock-outs and dominant-negative genetics in Trypanosoma
444 brucei. *Mol. Biochem. Parasitol.* **99**, 89–101 (1999).

445 55. Shanmugasundram, A. *et al.* TriTrypDB: An integrated functional genomics resource for
446 kinetoplastida. *PLoS Negl. Trop. Dis.* **17**, e0011058 (2023).

447 56. Ramírez, F. *et al.* deepTools2: a next generation web server for deep-sequencing data
448 analysis. *Nucleic Acids Res.* **44**, W160–W165 (2016).

449 57. Moloo, S. K. An artificial feeding technique for Glossina. *Parasitology* **63**, 507–512
450 (1971).

451 58. MacLeod, E. T., Maudlin, I., Darby, A. C. & Welburn, S. C. Antioxidants promote
452 establishment of trypanosome infections in tsetse. *Parasitology* **134**, 827–831 (2007).

453 59. Barnett, S. A. THE SKIN AND HAIR OF MICE LIVING AT A LOW
454 ENVIRONMENTAL TEMPERATURE. *Q. J. Exp. Physiol. Cogn. Med. Sci.* **44**, 35–42
455 (1959).

456

457 **Methods:**

458 Intravenous mouse infections and sample collection

459 Female C57Bl/6J (WT, strain# 000664 Jackson Laboratory) or B6.129P2-
460 *Aicda*$^{tm1(cre)Mnz}$/J (AID$^{-/-}$, strain# 007770 Jackson Laboratory)[42] between 7-10 weeks old were
461 each infected by intravenous tail vein injection with ~5 pleiomorphic EATRO 1125 AnTat1.1E
462 90-13 *T. brucei* parasites[24]. Blood parasitemia was counted by tail bleed every 2 days starting on
463 day 4 post-infection (PI) by hemocytometer with a limit of detection of 2.22×10^5 parasites/mL.
464 Blood (25uL) was collected by a submandibular bleed on days 6, 10, and 14 PI and placed into
465 TRIzol LS. For WT mice, 4 Mice were anesthetized and perfused at days 6, 10, and 14 PI.
466 Infected AID$^{-/-}$ mice were anesthetized and perfused at days 6 (2 mice) and 13 (3 mice) PI. Mice
467 were perfused with 50mL of PBS-Glucose (0.055M D-glucose) with heparin. After perfusion,

468 tissues were dissected and placed immediately into 1mL of RNA Later. The heart, lungs, gonadal
469 fat, subcutaneous fat, brain, and skin (ear) were collected.
470 For flow cytometry, immunofluorescence experiments, and single-cell sorting
471 experiments, 7-10 week old female C57Bl/6J mice were infected by intravenous tail vein
472 injection with ~5 AnTat1.1E chimeric triple reporter *T. brucei* parasites which express
473 tdTomato[35]. Blood was collected by a submandibular bleed at designated timepoints. For flow
474 cytometry, mice were anesthetized and perfused on days 6 and 13 P.I. as discussed above and the
475 gonadal fat and lungs were harvested. For immunofluorescence experiments, perfused tissues
476 were collected at day 13 P.I. For single-cell sorting, blood and tissues were only collected on day
477 14 P.I. All animal studies were approved by the Johns Hopkins Animal Care and Use Committee
478 (protocol # MO22H163).
479
480 VSG-seq sample and library preparation
481 RNA was isolated from blood samples stored in TRIzol LS (ThermoFisher, 10296010)
482 by phenol/chloroform extraction. Tissue samples were weighed and homogenized in TRIzol, and
483 then RNA was isolated by phenol/chloroform extraction. RNA from each sample was DNase
484 treated using Turbo DNase and cleaned up with Mag-Bind® TotalPure NGS beads (Omega Bio-
485 Tek M1378-00). First-strand cDNA synthesis was performed using SuperScript III Reverse
486 Transcriptase and a primer that binds to the conserved VSG 14-mer in the 3′-UTR (5'-
487 GTGTTAAAATATATC-3'). Products were cleaned up using Mag-Bind® TotalPure NGS beads
488 (Omega Bio-Tek, M1378-01). Next, a VSG-specific PCR with Phusion polymerase
489 (ThermoFisher, F530L) was performed using primers for the spliced leader (5'-
490 ACAGTTTCTGTACTATATTG-3') and SP6-VSG 14-mer sequences (5'-
491 GATTTAGGTGACACTATAGTGTTAAAATATATC-3') for 25 cycles. VSG-PCR products
492 were cleaned up using Mag-Bind® TotalPure NGS beads and quantified using the QuBit HS
493 DNA kit (Life Technologies). Finally, sequencing libraries were prepared with the Nextera XT
494 DNA Sample Prep Kit (Illumina) using the manufacturer's guidelines, and libraries were
495 sequenced with 100bp single-end reads on an Illumina HiSeq 2500.
496
497 Tissue-load and PAD1 QPCRs
498 First-strand synthesis was performed with SuperScript III Reverse Transcriptase (Thermo
499 Fisher Scientific, 18080051) and random hexamers primers on tissue RNA samples. QPCR was
500 performed in triplicate using SYBR Green qPCR Master Mix (Invitrogen, 4309155). tbZFP3
501 primers were used to estimate parasite load in tissue samples (FW: 5'-
502 CAGGGGAAACGCAAAACTAA-3'; RV: 5'-TGTCACCCCAACTGCATTCT-3'). CT values
503 were averaged between the triplicates and parasite load per mg of tissue were estimated using a
504 standard curve of values from RNA isolated from known numbers of cultured parasites
505 (Standard curves can be found in Extended Data Fig. 3d).
506 For PAD1 expression quantification, RNA extraction, first-strand synthesis, and QPCR
507 were performed following the same methods as above. PAD1 expression was quantified by
508 normalizing to tbZFP3 as a control gene (same primers as above) (PAD1 primers; FW: 5'-
509 CAGCGGCGATTATTGCATTGG-3'; RV: 5'- AGGAAGAAGGTTCCTTTGGTC-3'). CT
510 values were averaged between the triplicates and samples were compared using the delta-CT
511 between PAD1 and tbZFP3.
512
513 VSG-seq analysis

514 Analysis of sequencing results was performed following the method we reported
515 previously[7], with two changes: no mismatches were allowed for bowtie alignments and each
516 sample was analyzed (assembly, alignment, and quantification) separately. To compare
517 expressed VSG sets between samples, all assembled VSGs were clustered using CD-HIT-EST[51].
518 VSGs with >98% identity to one another were conservatively treated as one VSG. VSGs were
519 then identified by their Cluster number for further analysis. Samples that had less than 100,000
520 successfully aligning reads to VSGs were excluded from further analysis. Four samples, 3 brain
521 and 1 heart, were discarded because fewer than 100,000 reads aligned to VSG (Extended Data
522 Fig. 3a). Downstream analysis of expression data and generation of figures was performed in R.
523
524 Analysis of VSG sequence motifs
525 To identify whether there were tissue-specific VSG sequence motifs, the similarity of N
526 terminal sequences from all assembled VSGs were compared. N terminal sequences were
527 identified using a HMMEr scan against a database curated by Cross et al[2,52]. All N termini were
528 compared in an all vs all blast using default parameters. All VSG pairwise comparisons with an
529 e-value higher than 1E-3 were considered sufficiently similar to one another for further analysis.
530 VSGs that were found in a given tissue were binned into that tissue group, and the distribution of
531 the BLAST bitscores in a given compartment was compared against the total population of
532 similar VSGs.
533
534 Flow Cytometry
535 Once mice were perfused, tissues were dissected and washed with HBSS (Hanks
536 balanced salt solution, ThermoFisher Scientific 14175095). Tissue samples were minced and
537 placed in DMEM (ThermoFisher Scientific, 11995065) containing either 1 mg/mL collagenase
538 type 1 (ThermoFisher Scientific, 17100017) for adipose fat or 2 mg/mL collagenase type 2
539 (ThermoFisher Scientific, 17101015) for lung samples. Hearts were dissociated using 2 mg/mL
540 collagenase type 2, 50U/mL DNase I, and 20U/mL Hyaluronidase. These were then incubated in
541 a 37°C water bath for 1 hour and briefly vortexed every 10 minutes. Next, samples were passed
542 through a 70µM filter and centrifuged at 2600 x g for 8 mins at 4 C, and the cell pellet was taken
543 for antibody staining.
544 Blood samples were collected by submandibular bleed and red blood cells were depleted
545 by magnetic-activated cell sorting (MACS) with anti-Ter-119 MicroBeads (Miltenyi Biotech,
546 130-049-901) following the manufacturer's protocol. Cells were pelleted and washed with HMI-
547 9 media.
548 All samples, both blood and tissues, were stained with Zombie Aqua™ dye at 1:100 in
549 PBS and washed with PBS following the manufacturer's protocol (BioLegend, 423101).
550 Samples were then stained for 10 minutes at 4°C with a rabbit anti-AnTat1.1 polyclonal antibody
551 diluted 1:15,000 in HMI-9 media and washed once with HMI-9 (antibody courtesy of Jay
552 Bangs). Then, secondary antibody staining was performed while shaking for 10 minutes at 4°C
553 with Anti-Rabbit IgG (H+L), F(ab')2 Fragment conjugated to Alexa Fluor® 488 fluorescent dye
554 (Cell Signaling Technology, 4412S). Finally, samples were washed with cold PBS and
555 resuspended in PBS for flow cytometry analysis. Samples were run on a Beckton Dickenson A3
556 Symphony flow cytometer and analysis was performed using FlowJo (version 10.6.1) (see
557 Extended Data Fig. 7a for gating strategy).
558
559 Immunofluorescence

560 Mice infected with AnTat1.1E chimeric triple reporter *T. brucei* parasites that express
561 tdTomato were sacrificed and perfused as previously described at days 6 and 13 PI. Lung, heart,
562 and gonadal fat were collected and fixed in 4% paraformaldehyde in PBS for 12 hours at 4 C.
563 Post-fixation, tissues were frozen, embedded in O.C.T. Compound (Tissue-Tek), and cut by
564 cryostat microtome into 10µm sections.
565 The following antibodies were applied to sections: rat anti-mouse CD31 (PECAM-1)
566 (SCBT) with goat anti-rat Fluor 488 (CST). Coverslips were mounted using ProLong Gold (Life
567 technologies). Tissues were imaged with 4x, 10x, and 20x objectives using a Nikon Eclipse 90i
568 fluorescence microscope (Nikon) and X-Cite 120 fluorescent lamp (Excelitas) with an ORCA-
569 ER digital CCD camera (Hammamatsu) and ImageJ v1.53 image analysis software. Image
570 collection and analysis followed published guidelines for rigor and reproducibility[53].
571
572 Serum antibody ELISA quantification
573 Blood (25uL) was collected by submandibular bleed on days 0, 6, 10, and 14 PI from
574 mice infected with ~5 pleiomorphic EATRO 1125 AnTat1.1E 90-13 *T. brucei* parasites. Serum
575 was isolated using serum separator tubes (BD Microtainer SST tubes, 365967). IgM and IgG
576 were quantified by ELISA using ThermoFisher IgM and IgG kits following manufacturer
577 protocols (IgG cat# 88-50400-88, IgM cat# 88-50470-88).
578
579 Serum sample flow cytometry on *T. brucei*
580 Blood was collected from 2 mice infected with AnTat1.1E chimeric triple reporter *T.*
581 *brucei* parasites, which initially express the VSG AnTat1.1, by cheek bleed. Serum was isolated
582 by spinning blood samples at 10,000xg for 5 mins and pipetting off the top serum layer. EATRO
583 1125 AnTat1.1E 90-13 *T. brucei* parasites[24] expressing the VSG AnTat1.1 and Monomorphic
584 Single Marker Lister427 VSG221 TetR T7RNAP bloodstream form (NR42011; LOT:
585 61775530)[54], which express VSG-2, were used for flow cytometry. 10^6 Parasites were stained in
586 duplicate while shaking for 10 minutes at 4°C using mouse serum diluted 1:100 in PBS. As a
587 positive control, a rabbit anti-AnTat1.1 polyclonal antibody diluted 1:15,000 in PBS was used
588 following the same staining procedure (antibody courtesy of Jay Bangs). Then, secondary
589 antibody staining was performed while shaking for 10 minutes at 4°C with Anti-mouse IgG
590 (H+L), F(ab')2 Fragment conjugated to Alexa Fluor® 647 fluorescent dye (Cell Signalling
591 Technology, 4410S) or Anti-Rabbit IgG (H+L), F(ab')2 Fragment conjugated to Alexa Fluor®
592 647 fluorescent dye (Cell Signaling Technology, 4414S). Finally, samples were washed with
593 cold PBS and resuspended in PBS for flow cytometry analysis. Samples were run on an Attune
594 Nxt flow cytometer (Invitrogen) and analysis was performed using FlowJo (version 10.6.1).
595
596 Single-cell sorting and RNA-seq library preparation
597 Blood and tissue samples (heart, gonadal fat, and lung) from two mice were collected
598 after perfusion as described above. For sorting parasites, the same tissue dissociation and flow
599 cytometry was performed as described above, with the exception of live/dead staining, which
600 was performed using propidium iodide instead of Zombie Aqua™. Samples were kept on ice as
601 much as possible through this process. Single live, tdTomato$^+$ *T. brucei* cells were sorted into
602 chilled 384-well plates for SL-Smart-seq3xpress library preparation containing lysis buffer and
603 an RNA spike-in control using a Beckman Coulter MoFlo™ XDP cell sorter (see Extended Data
604 Fig. 7b for gating strategy). For each blood and tissue sample a single plate of parasites were
605 sorted for a total of 370 cells per sample.

606 The SL-Smart-seq3xpress library preparation approach was followed as described in
607 McWilliam et al[33]. Briefly, single cells were lysed by incubation at 72°C for 10 minutes in 0.3 µl
608 of lysis buffer. Reverse transcription was done by adding 0.1µl of reverse transcription mix to
609 each well and incubation at 42°C for 90 minutes, followed by ten cycles of 50°C for 2 minutes
610 and 42°C for 2 minutes, with a final incubation at 85°C for 5 minutes. Preamplification was done
611 by adding 0.6µl of a mix containing primers annealing to the Spliced-Leader sequence and to a
612 conserved sequenced added by the oligodT primer during retrotranscription, with the following
613 cycling conditions: 95°C for 1 minute, 16 cycles of : 98°C for 10 seconds, 65°C for 30 seconds,
614 68°C for 4 minutes; and final 72°C for 10 minutes. Following, the amplified cDNA was diluted
615 by adding 9µl of water per well. Next, 1 µl of each well was transferred to a new plate, 1µl of
616 tagmentation mix was added and the plate incubated at 55°C for 10 minutes for tagmentation.
617 The reaction was stopped by adding 0.5µl of 0.2% SDS to each well and incubating for 5
618 minutes. The final index PCR was done by adding 1µl of specific index primer combinations to
619 each well and 1.5µl of PCR mix. The following cycling conditions were used: 72° for 3 minutes,
620 95°C for 30 seconds, 14 cycles of: 95°C for 10 seconds, 55°C for 30 seconds, 72°C for 1 minute;
621 followed by 72°C for minutes. Single-cell libraries were then pooled and purified using AMPure
622 XP beads at a ratio of 1:0.7. Libraries were run on a 4% non-denaturing PAGE gel and purified
623 according to standard polyacrylamide gel purification protocols. Purified libraries from multiple
624 plates were pooled and sequenced on a NextSeq 1000 sequencing platform to produce paired-end
625 reads of 101nt (cDNA) and 19nt (TAG+UMI read), and 8nt for the index reads.
626
627 Single-cell RNA-seq primary processing and VSG de novo assembly
628 The primary processing of the sequencing data was as described in McWilliam et al[33].
629 Briefly, the two reads containing the indexes (8nt each) and the one containing the TAG+UMI
630 (19nt) were concatenated into a 35nt read. Artifact reads containing the TAG sequence (or its
631 reverse complement) in the cDNA reads were filtered out with Cutadapt.
632 For analysis of derepression by *de novo* assembly of VSGs, the filtered reads were sorted
633 into individual files for each cell, and these read files were run through our VSG-Seq analysis
634 pipeline individually using the same parameters as described above for bulk VSG-Seq. Using
635 this approach, VSG open reading frames (ORFS) were assembled and quantified for each cell
636 individually. VSG ORFs were then clustered among all single cells (VSG clusters were not
637 related to previous VSG clusters from bulk VSG-seq and cannot be compared to the previous
638 analysis based on cluster names).
639 For analysis of derepression by alignment to the genome, filtered reads were mapped
640 with STAR (version 2.7.10a) to a hybrid fasta file combining the *T. brucei* EATRO 1125 strain
641 genome assembly (version 67, downloaded from TriTrypDB[55]) and the set of 10 sequences used
642 as RNA spike-in. The count matrix obtained was then corrected with the index hopping filtering
643 pipeline "scSwitchFilter" (https://github.com/colomemaria/scSwitchFilter). Only cells with at
644 least 500 genes detected, 1000 gene UMI transcript counts, 30 spike-in UMI counts, and 10 VSG
645 UMI counts were used for downstream analyses. A total of 1216 total cells fit these criteria out
646 of 2960 total cells sequenced. For each tissue and blood sample a single plate (370 cells) was
647 sequenced. For assessment of potential derepression (Extended Data Figure 5b,e), VSGs with >1
648 UMI count were considered expressed in a cell. Cells were considered to be monogenically
649 expressing a VSG (Extended Data Figure 5e) if the VSG represented ≥80% of VSG UMI counts.
650 For evaluating read coverage of VSGs and VSG clusters, Bowtie indexes were created
651 for each reference sequence then reads from a single cell were aligned using Bowtie1. Read

652 coverage was calculated using deepTools[56] to convert BAM alignment files to bigWig coverage
653 tracks. Coverage was then visualized using the ggcoverage package in R
654 (https://github.com/showteeth/ggcoverage).
655
656 Tsetse fly husbandry and fly bite-inoculated mouse infections
657 *Glossina morsitans morsitans* were maintained in the Yale School of Public Health
658 insectary at 25°C with 65-70% relative humidity under a 12h:12h light:dark photoperiod. All
659 flies received defibrinated sheep blood (Lampire Biologicals) every 48 hours through an artificial
660 membrane feeding system[57]. Newly eclosed adult female flies were administered *per os* an initial
661 blood meal containing $1x10^6$/ml of *Trypanosoma brucei brucei* (strain RUMP 503; previously
662 expanded in rats) and cysteine (10µM; to increase the infection prevalence; [58]). After this single
663 parasite challenge, flies were maintained on normal blood every other day.
664 Thirty-five days post-challenge (the time it takes *T. b. brucei* to complete their
665 developmental cycle within the tsetse fly and become infectious to a new vertebrate host), six to
666 eight-week-old female C57Bl/6J mice were exposed to the bite of individual, trypanosome
667 challenged flies 72 hrs after the flies had taken their last blood meal. Following the consumption
668 of mouse blood, individual flies were microscopically dissected to confirm that their salivary
669 glands were infected with vertebrate-infectious metacyclic stage *T. b. brucei* (if not, another fly
670 was allowed to feed on the mouse until it was confirmed that an infectious fly had taken a blood
671 meal). Five mice were infected using this method. All experiments using mice were performed in
672 strict accordance with the Yale University Institutional Animal Care and Use Committee policies
673 (Protocol 2014–07266 renewed on March 2023).
674 Once mice were infected, blood parasitemia was counted by tail bleed every 2 days
675 starting on day 4 post-infection (PI) by hemocytometer with a limit of detection of $2.22x10^5$
676 parasites/mL. Blood (25uL) was collected by a submandibular bleed on days 6, 10, and 14 PI and
677 placed into TRIzol LS. Five Mice were anesthetized and perfused at day 14 PI. Mice were
678 perfused with 50mL of PBS-Glucose (0.055M D-glucose) with heparin. After perfusion, tissues
679 were dissected and placed immediately into 1mL of RNA Later. The heart, lungs, gonadal fat,
680 subcutaneous fat, brain, and skin (ear) were collected. Sequencing libraries were prepared and
681 analyzed following the methodology described above.
682 To quantify the mVSG repertoire of RUMP 503, we also collected a pool of tsetse saliva
683 containing RUMP 503 *T. brucei* parasites. This sample was stored in TRIzol LS, RNA was
684 extracted, and the sample was prepared for sequencing as described above. The VSG-Seq
685 pipeline was used to quantify mVSG expression in the sample.
686
687 Statistics and figures
688 Normality was tested for all Students t-tests and Dunnet's tests analyses and can be found
689 in the code on the repository at https://github.com/mugnierlab/Beaver2022. Nearly all VSG
690 diversity measurements were found to be normally distributed, except for some samples with low
691 VSG counts or sample numbers. We thus assumed normality for all VSG diversity
692 measurements. All reported P-values have been corrected for multiple comparisons using the
693 Benjamini–Hochberg procedure. For all figures with boxplots, the box represents the first (25%)
694 and third (75%) quartiles with a line at the median. Extending lines represent the maximum and
695 minimum values not including outliers that are further than 1.5 times the interquartile range from
696 either end of the box.
697

Data availability:

Code and data for generating the analysis and figures in this paper are available at https://github.com/mugnierlab/Beaver2022. Raw sequencing data are available in National Center for Biotechnology Information (NCBI) Sequence Read Archive under accession number PRJNA858046.

Methods references:

2. Cross, G. A. M., Kim, H. S. & Wickstead, B. Capturing the variant surface glycoprotein repertoire (the VSGnome) of Trypanosoma brucei Lister 427. *Mol. Biochem. Parasitol.* **195**, 59–73 (2014).

7. Mugnier, M. R., Cross, G. A. M. & Papavasiliou, F. N. The in vivo dynamics of antigenic variation in Trypanosoma brucei. *Science* **347**, 1470–3 (2015).

25. Engstler, M. & Boshart, M. Cold shock and regulation of surface protein trafficking convey sensitization to inducers of stage differentiation in Trypanosoma brucei. *Genes Dev.* **18**, 2798 (2004).

28. Calvo-Alvarez, E., Cren-Travaillé, C., Crouzols, A. & Rotureau, B. A new chimeric triple reporter fusion protein as a tool for in vitro and in vivo multimodal imaging to monitor the development of African trypanosomes and Leishmania parasites. *Infect. Genet. Evol.* **63**, 391–403 (2018).

29. Robbiani, D. F. *et al.* Activation Induced Deaminase is required for the chromosomal breaks in c-myc that lead to c-myc/IgH translocations. *Cell* **135**, 1028 (2008).

33. McWilliam, K. R. *et al.* High-resolution scRNA-seq reveals genomic determinants of antigen expression hierarchy in African Trypanosomes. *bioRxiv* 2024.03.22.586247 (2024). doi:10.1101/2024.03.22.586247

36. Fu, L., Niu, B., Zhu, Z., Wu, S. & Li, W. CD-HIT: accelerated for clustering the next-generation sequencing data. *Bioinformatics* **28**, 3150 (2012).

37. So, J. *et al.* Trypanosomal variant surface glycoprotein expression in human African trypanosomiasis patients. *bioRxiv* 2021.09.09.459620 (2021). doi:10.1101/2021.09.09.459620

38. Lee, J.-Y. & Kitaoka, M. A beginner's guide to rigor and reproducibility in fluorescence imaging experiments. *https://doi.org/10.1091/mbc.E17-05-0276* **29**, 1519–1525 (2018).

49. Shanmugasundram, A. *et al.* TriTrypDB: An integrated functional genomics resource for kinetoplastida. *PLoS Negl. Trop. Dis.* **17**, e0011058 (2023).

50. Moloo, S. K. An artificial feeding technique for Glossina. *Parasitology* **63**, 507–512 (1971).

51. MacLeod, E. T., Maudlin, I., Darby, A. C. & Welburn, S. C. Antioxidants promote establishment of trypanosome infections in tsetse. *Parasitology* **134**, 827–831 (2007).

Acknowledgments: We would like to thank Jay Bangs for supplying us with the anti-AnTat1.1 antibody and Brice Rotureau for providing us with the chimeric triple reporter cell line. We thank Tricia Nilles and Worod Allak at the Becton Dickinson Immunology and Flow Cytometry

core at Johns Hopkins Bloomberg School of Public Health for training, support, and technical assistance using the BD FACS Symphony A3. We would like to also thank Hao Zhang and Joseph Margolick from the Flow Cytometry Cell Sorting Core Facility at Bloomberg School of Public Health, Johns Hopkins University for doing FACS sorting. The facility was supported by CFAR: 5P30AI094189-04 (Chaisson), 1S10OD016315-01 and 1S10RR13777001. Data analysis was carried out at the Advanced Research Computing at Hopkins (ARCH) core facility (rockfish.jhu.edu), which is supported by the National Science Foundation (NSF) grant number OAC 1920103. AKB was supported by NIH T32AI007417. NPC was supported by NIH T32 OD011089. FR-F is supported by NIH NIGMS 1K99GM132557-01 and is an Investigator in the Chan Zuckerberg Biohub. MRM, AKB, JES, NPC, JMCH, BB, and BZ were supported by Office of the Director, NIH (DP5OD023065). In addition, this study was funded by the German Research Foundation [SI 1610 / 2-2] and an ERC Consolidator Grant (SwitchDecoding 101044320) awarded to TNS. ZK was supported by a MSCA ITN Cell2Cell fellowship.

Author contributions:

Conceptualization: AKB, MRM, LMF, FRF, TNS, ROC, SA, BLW

Methodology: AKB, ROC, ZK, BLW, EOA, GMS, NPC, GYB, JMCH, JES, BZ, BB

Investigation: AKB, ROC, ZK, BLW, NPC, GYB, JH, JES

Visualization: AKB, NPC, JMCH

Funding acquisition: MRM, LMF, TNS, SA

Project administration: MRM

Supervision: MRM

Writing – original draft: AKB, MRM

Writing – review & editing: AKB, JES, GYB, BZ, MRM, FRF, LMF, TNS, ROC

Competing interests: The authors declare that they have no competing interests.

Materials and correspondence: Correspondence and requests for materials should be addressed to Monica Mugnier (mmugnie1@jhu.edu).

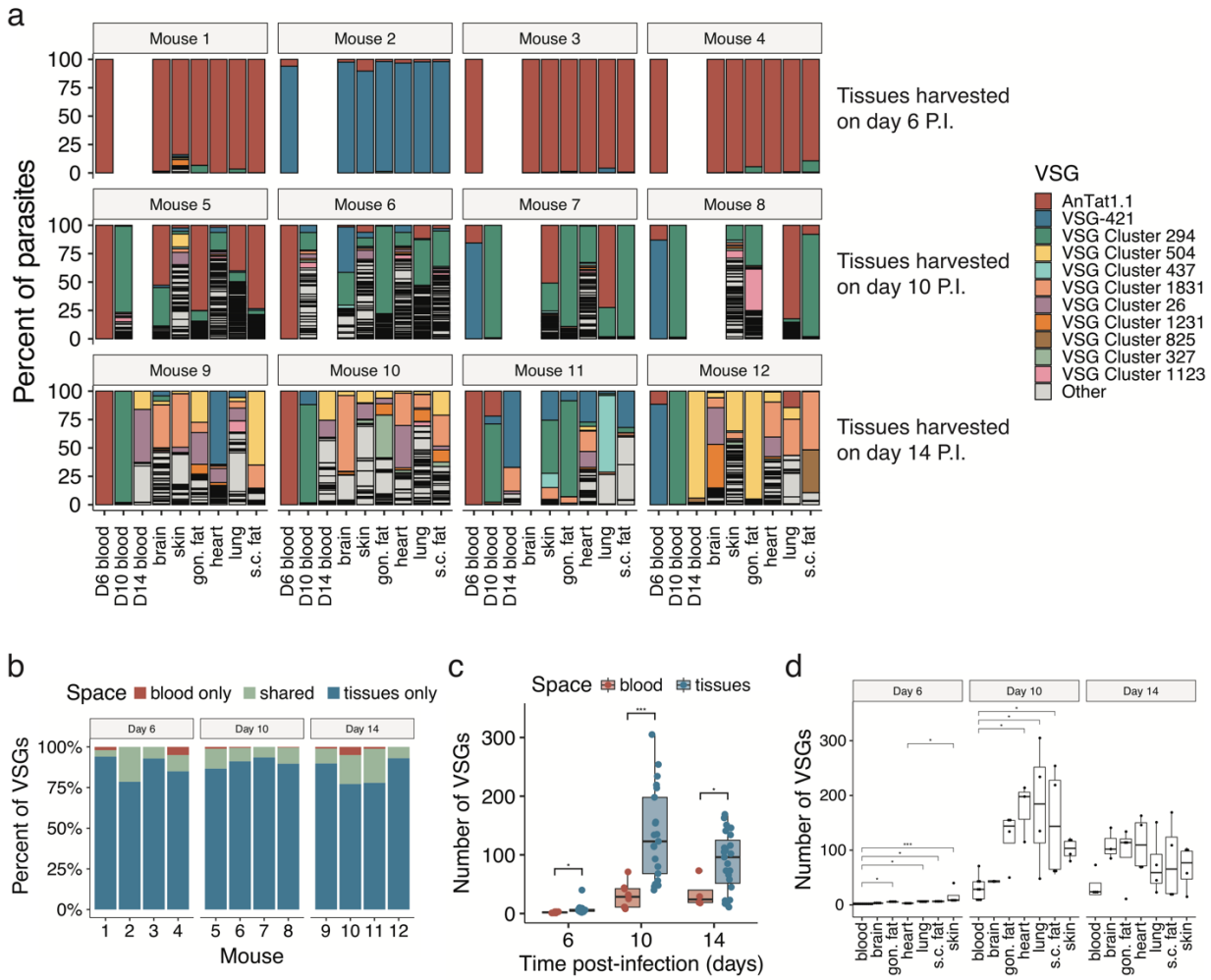

Fig. 1. Extravascular parasites harbor most of the antigenic diversity in an infection. (**a**) The percentage of parasites expressing each VSG within a space. The 11 VSGs with the highest overall expression are colored, and all other VSGs are in grey as "other". Gon. fat = gonadal fat, s.c. fat = subcutaneous fat, P.I. = post-infection. (**b**) Stacked bar graphs from each infected mouse representing the percentage of VSGs that were found exclusively within the blood (red), exclusively within tissue spaces (blue), or shared by both the blood and at least one tissue (green). (**c**) Quantification of the number of VSGs found within the blood (red) or tissue spaces (blue) at each time point (Shapiro-Wilk normality test followed by a two-tailed Student's t-test BH corrected). (**d**) The number of VSGs in each tissue space (Shapiro-Wilk normality test followed by a two-tailed Dunnett's test) (For statistical tests *P<0.05, ***P<0.001).

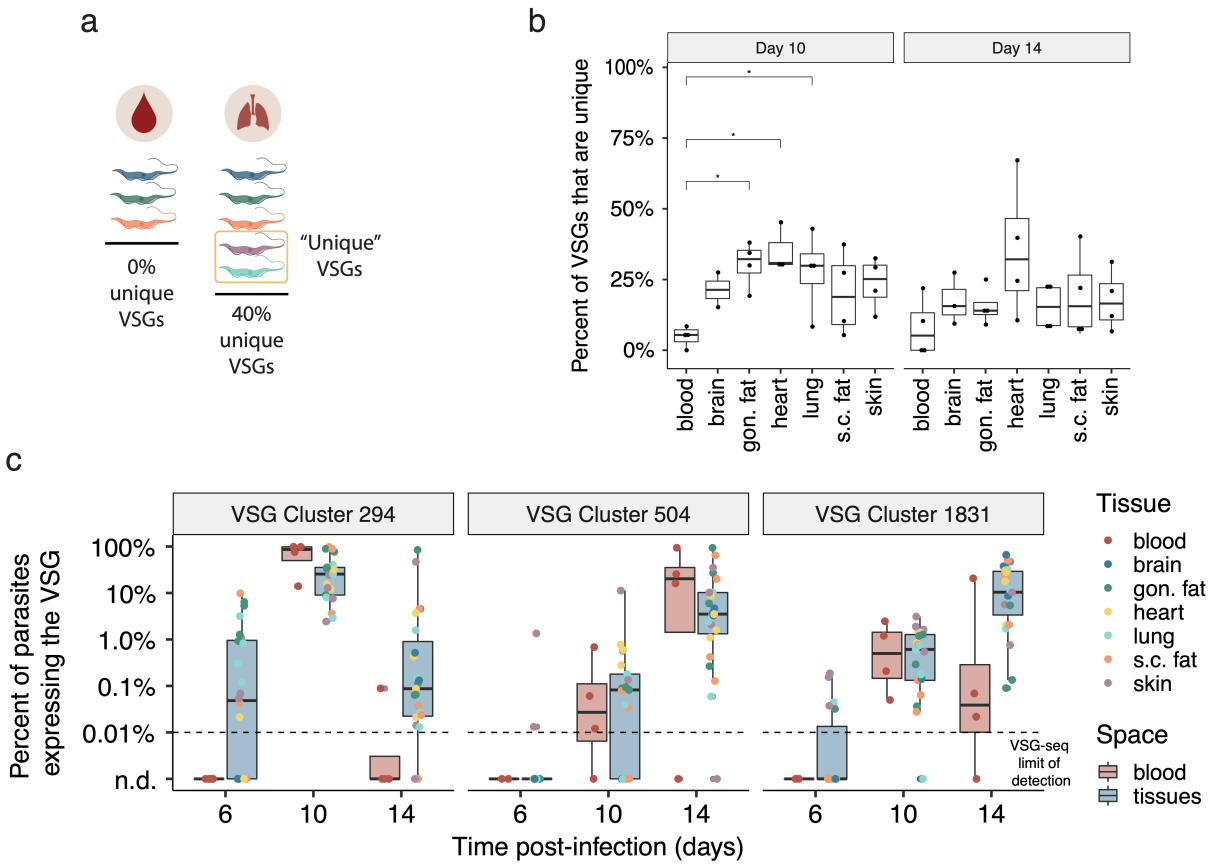

Fig. 2. Tissue-resident parasites express a unique repertoire of VSGs during infection. (**a**) We define "unique" VSGs as those VSGs solely found within a specific space in a mouse (Created with BioRender.com). (**b**) The percentage of VSGs that were unique to one space within a mouse (Shapiro-Wilk normality test followed by a two-tailed Dunnett's test, *P<0.05). Day 6 samples were excluded from this analysis because few VSGs are expressed at this point. Gon. fat = gonadal fat, s.c. fat = subcutaneous fat. (**c**) The expression of three representative VSGs (cluster 294, 504, and 1831) within blood and tissue samples on days 6, 10, and 14. "n.d" indicates that the VSG was not detected.

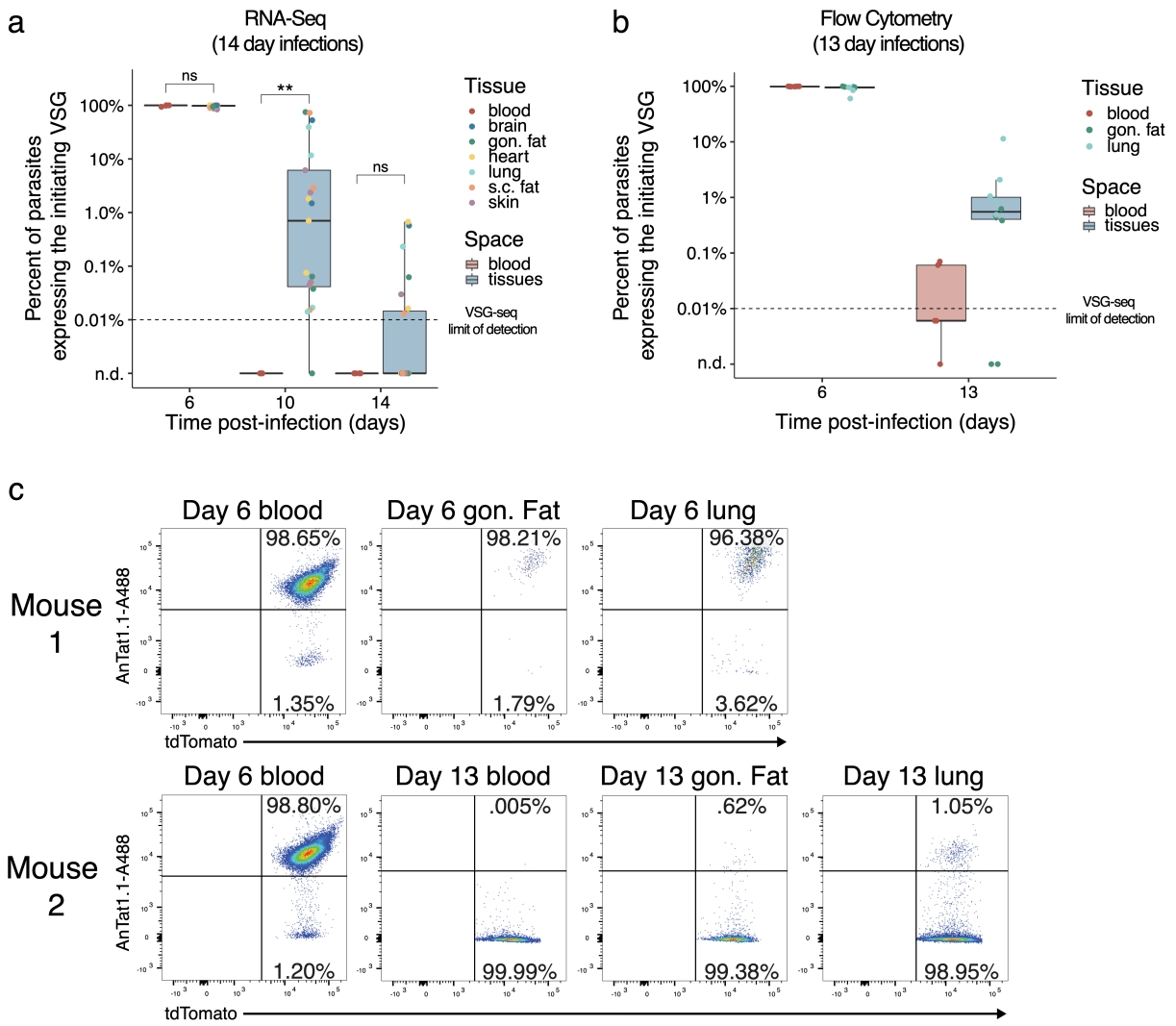

Fig. 3. VSG-specific parasite clearance is slower in tissues than in the blood. (**a**) The percentage of parasites expressing the initiating VSG (AnTat1.1 or VSG-421) at days 6, 10, and 14 post-infection. Tissue samples were grouped together (blue) and compared to blood samples (red) (two-tailed Wilcoxon test, ns = not significant, **P<0.01). "n.d" = not detected, gon. fat = gonadal fat, s.c. fat = subcutaneous fat. (**b**) Quantification of the number of parasites that were tdTomato positive and stained positive for AnTat1.1 by flow cytometry (n = 5 mice). The horizontal dotted line represents the limit of detection for VSG-seq. "n.d" indicates that the VSG was not detected. (**c**) Representative flow cytometry plots from tissues collected from mice infected with chimeric triple marker parasites that express tdTomato constitutively in their cytoplasm. Parasites were stained with anti-AnTat1.1 antibody.

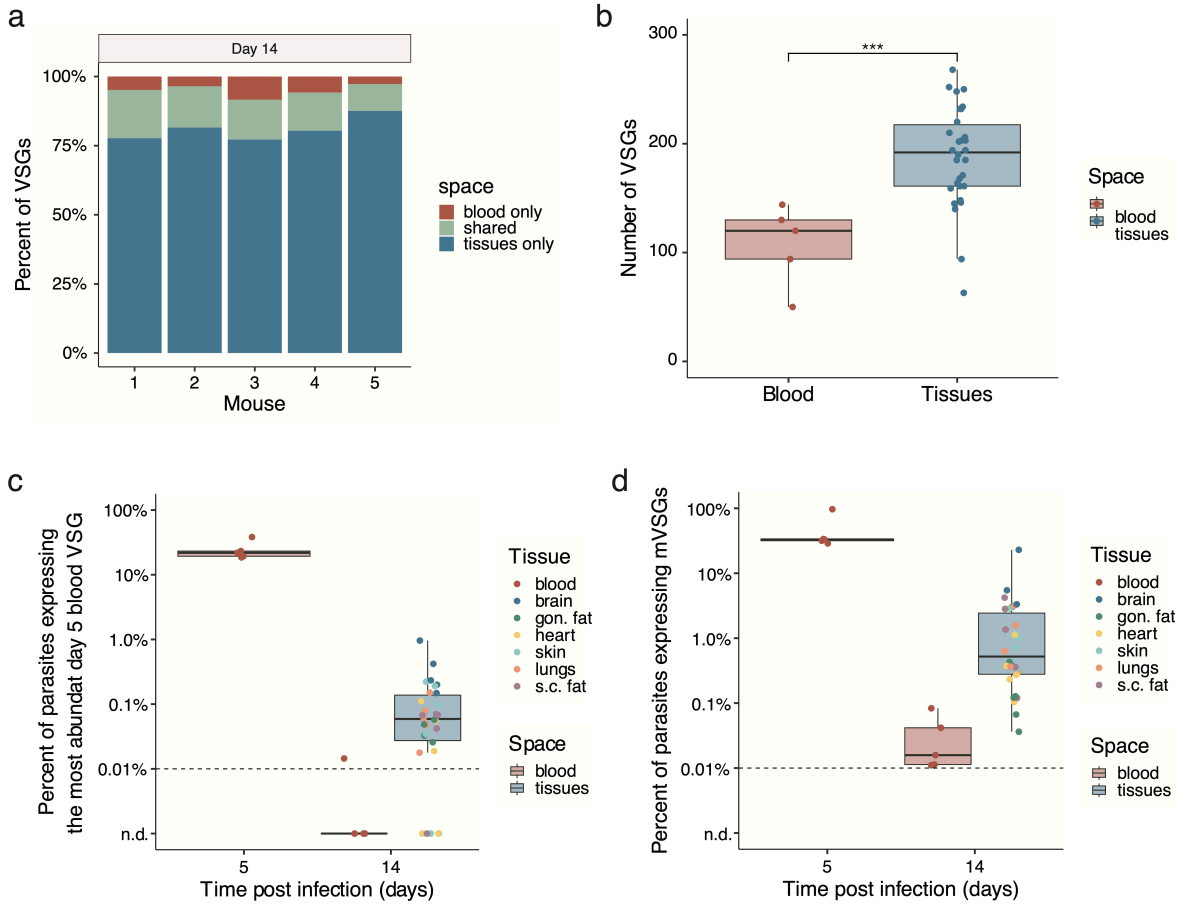

Fig. 4. Tsetse bite-initiated infections show increased antigenic diversity and delayed immune clearance in extravascular spaces. Data from five mice infected with RUMP 503 parasites from a tsetse fly bite. (**a**) Bar graphs representing the percentage of VSGs in each mouse that were found exclusively within the blood (red), exclusively within tissue spaces (blue), or shared by both the blood and at least one tissue (green). (**b**) Quantification of the number of VSGs found within the blood (red) or tissue spaces (blue) on day 14 post-infection (Shapiro-Wilk normality test followed by a two-tailed Student's t-test BH corrected, ***P<0.001). (**c**) The percentage of parasites within each mouse expressing the most abundant VSG from the day 5 blood. (**d**) The percentage of parasites expressing one of the mVSGs found to be expressed by RUMP 503 parasites in the salivary gland of a tsetse fly.

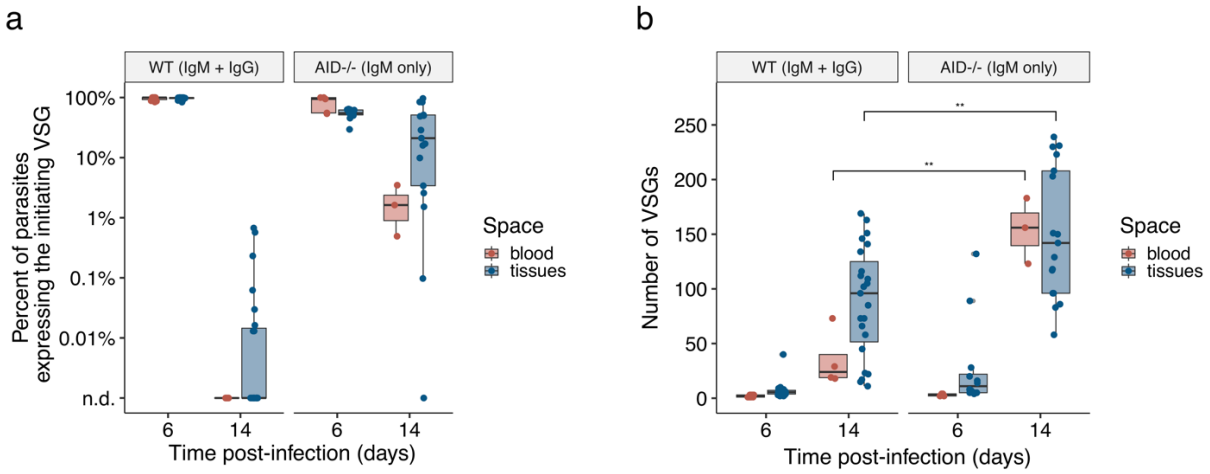

Fig. 5. Delayed parasite clearance correlates with an increase in VSG diversity. (**a**) The percentage of parasites expressing the initiating VSG (AnTat1.1 or VSG-421) in both WT and AID$^{-/-}$ mice. "n.d" indicates that the VSG was not detected. (**b**) The number of VSGs expressed within the blood (red) and tissues (blue) of WT and AID$^{-/-}$ mice (Shapiro-Wilk normality test followed by a two-tailed Student's t-test, **P<0.01).

Extended data:

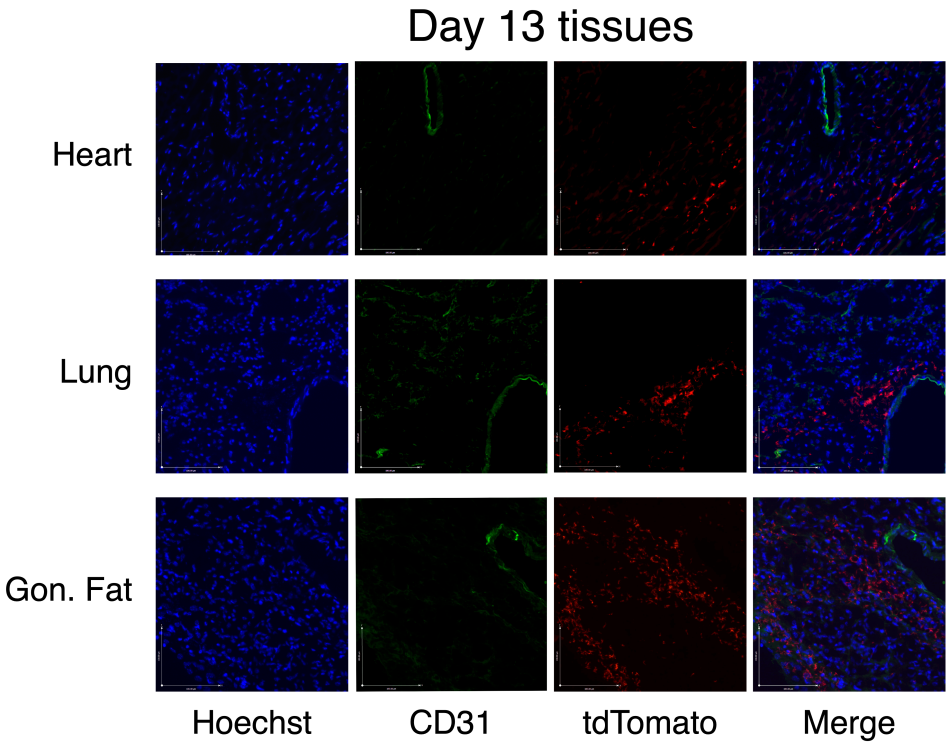

Extended Data Fig. 1. Immunofluorescence images of tdTomato expressing parasites (red) from cross sections of perfused tissues stained with hoechst (blue) and anti-CD31 antibody (green). TdTomato-positive parasites localized separately from CD31 lined spaces, showing that parasites are extravascular.

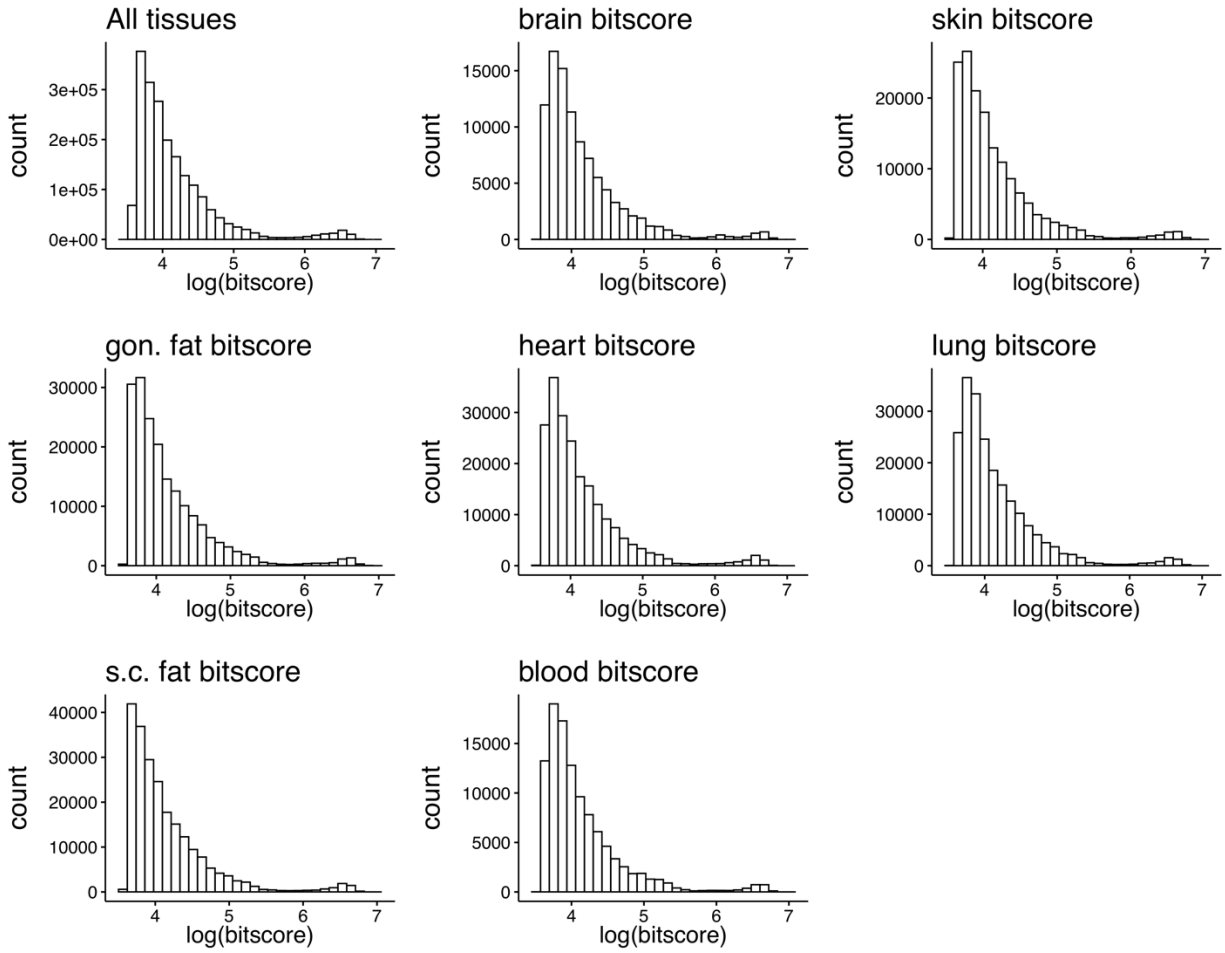

Extended Data Fig. 2. Distribution of bitscores across tissue compartments. The similarity of VSGs detected in each tissue as measured by bitscore, a sequence similarity metric normalized to the database size, allows for comparing tissue compartments with different numbers of total VSGs expressed in each tissue. No statistical significance was found.

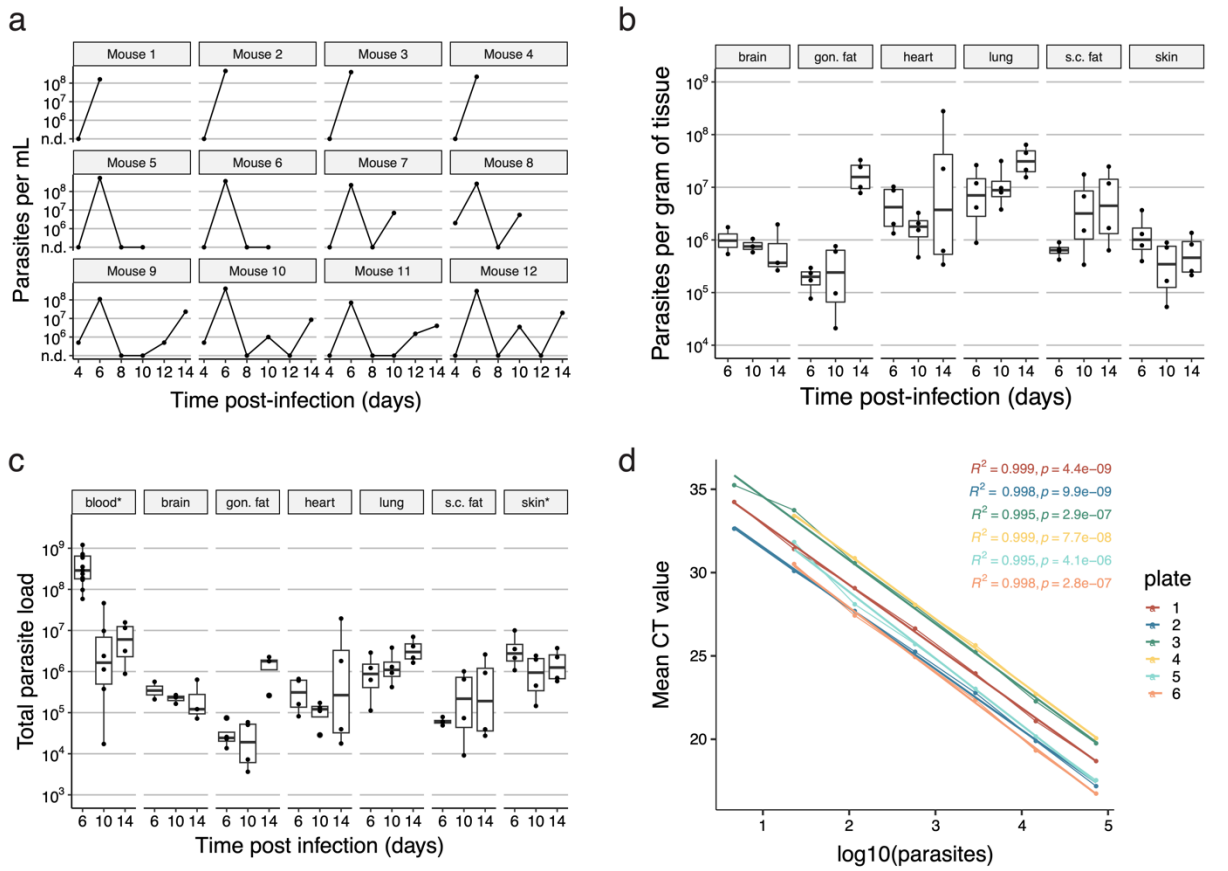

Extended Data Fig. 3. (**a**) Parasitemia of 12 mice infected with AnTat1.1E *T. brucei* counted from tail blood by hemocytometer ("n.d." = not detectable, limit of detection of 2.22×10^5 parasites/mL). (**b**) Estimated parasite load per gram of tissue using QPCR. tbZFP3 was used as the control and RNA from known quantities of parasites was used to make standard curves. (**c**) The approximate total number of parasites represented in each organ. This was calculated using the estimated number of parasites from QPCR and the recorded organ mass. For the blood and skin, it was assumed that each mouse had 1.5mL of blood and 2.73 grams of skin[59] to estimate the total load within these organs. (**d**) The qPCR standard curves used for each plate of samples. These were used to estimate the number of parasites represented in each of our tissue samples based on RNA from known parasite concentrations (cultured parasites counted using a hemocytometer).

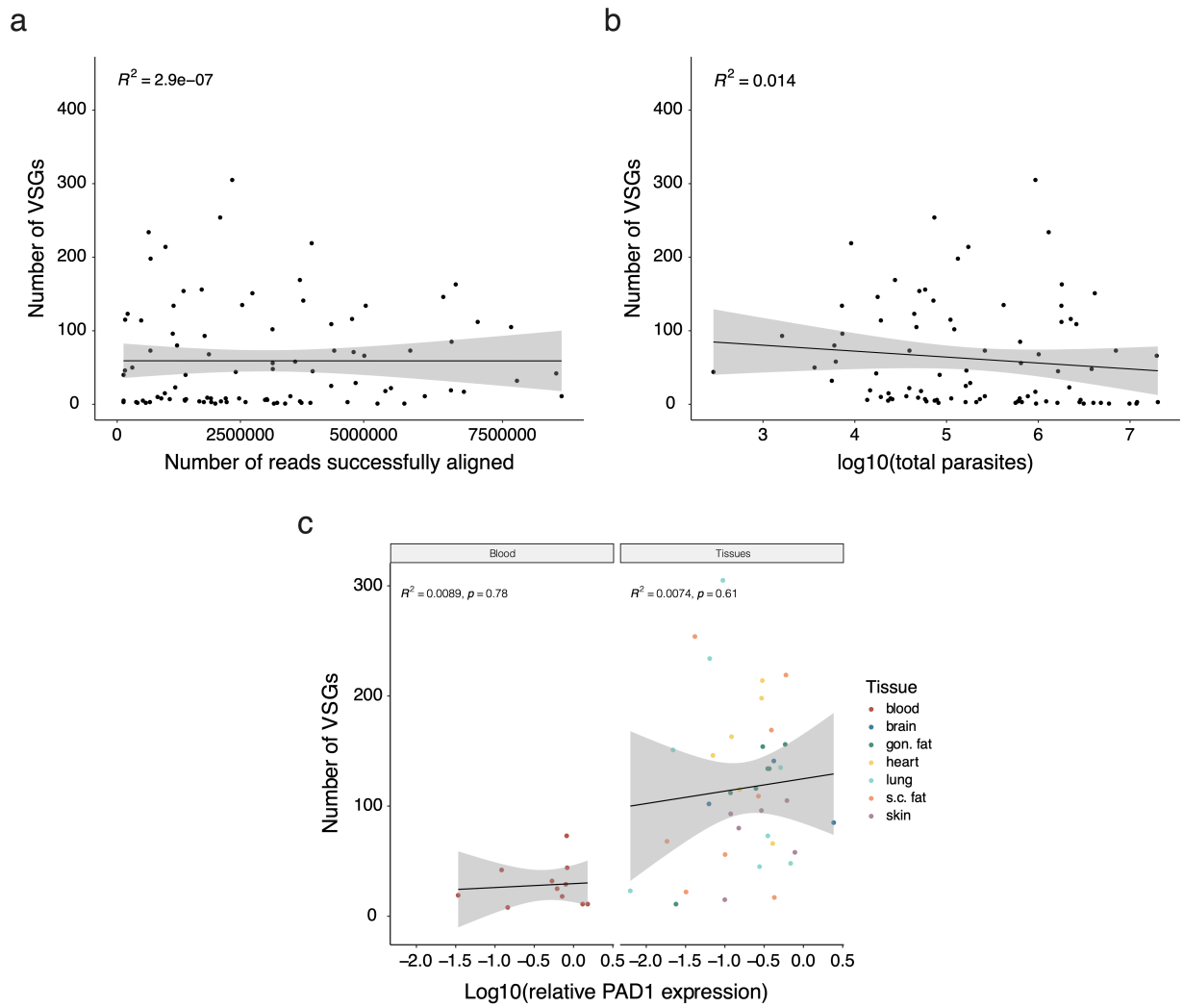

Extended Data Fig. 4. (**a**) A comparison of the number of reads successfully aligned in a sample and the number of VSGs observed. (**b**) A comparison of the total number of parasites and the number of VSGs found in each sample. (**c**) The correlation between PAD1 expression relative to the housekeeping gene tbZFP3 and the number of VSGs expressed at the population level for each sample.

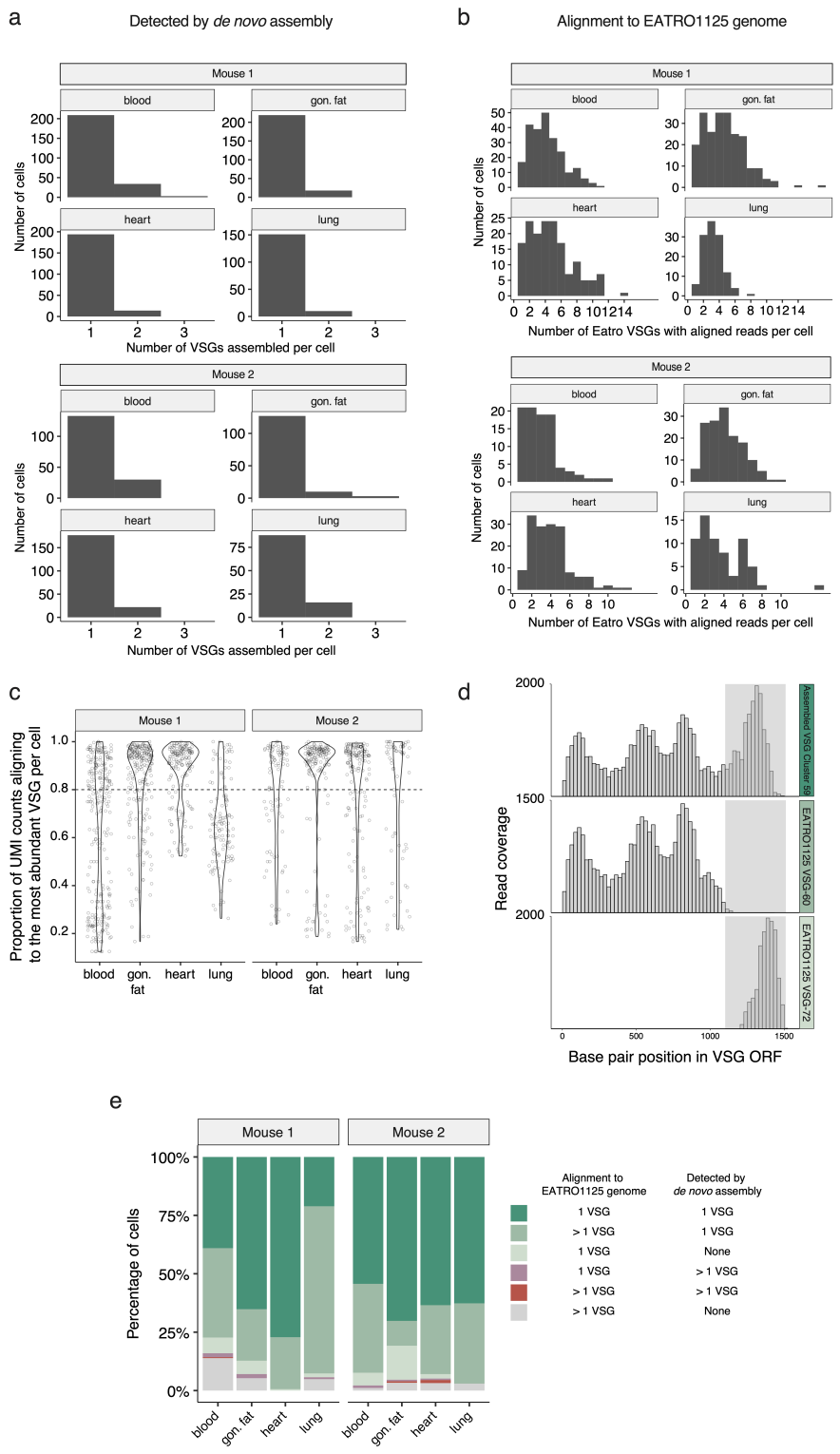

Extended Data Fig. 5. (**a**) The number of VSG open reading frames (ORFs) detected per cell by *de novo* assembly with the VSG-Seq pipeline. In this figure, all cells sequenced were evaluated for VSG ORF assembly without any filtering (1377 total cells had a *de novo* assembled VSG). (**b**) The number of EATRO1125 VSGs detected per single cell. Cells were evaluated for VSG

858 expression only if they had at least 500 genes detected, 1000 gene UMI counts, 30 spike-in UMI
859 counts, and 10 VSG UMI counts (1216 cells fit these criteria out of 2960 total sequenced cells).
860 Only VSGs with >1 UMI count were considered for quantification of VSG expression. (**c**)
861 Alignment to the EATRO1125 genome assembly was used to quantify the fraction of VSG UMI
862 counts coming from the most abundant VSG gene within each cell. The dashed line represents
863 the 0.8 fraction of total VSG UMI counts (80%) threshold set to define monogenic expression
864 with one dominant VSG in a cell. Only cells that had at least 500 genes detected, 1000 gene UMI
865 transcript counts, 30 spike-in UMI counts, and 10 VSG UMI counts were evaluated for this
866 analysis (1216 total cells out of 2960 total cells sequenced). (**d**) Representative histograms of
867 coverage for reads from one cell. Read coverage is shown for the *de novo* assembled VSG
868 cluster 59 and two genomic VSG ORFs, VSG-60 and VSG-72, which represent a common
869 scenario that creates ambiguous VSG expression if reads are only aligned to the EATRO1125
870 genome. Many cells in the Mouse 1 lung sample expressed this VSG and exhibited this mapping
871 problem. (**e**) The VSG expression classification for each cell using both methods (alignment to
872 the EATRO1125 genome and *de novo* assembly). In both alignment and assembly, if a VSG
873 represented 80% or more of the VSG UMI counts in a cell (for genomic mapping) or 80% of the
874 population (for VSG-seq analysis), that cell was considered to be expressing only the dominant
875 VSG. Only cells that had at least 500 genes detected, 1000 gene UMI transcript counts, 30 spike-
876 in UMI counts, and 10 VSG UMI counts were evaluated for this analysis (1216 cells fit these
877 criteria out of 2960 total cells sequenced). Only VSGs with >1 UMI count were considered for
878 quantification by alignment to the EATRO1125 genome.
879

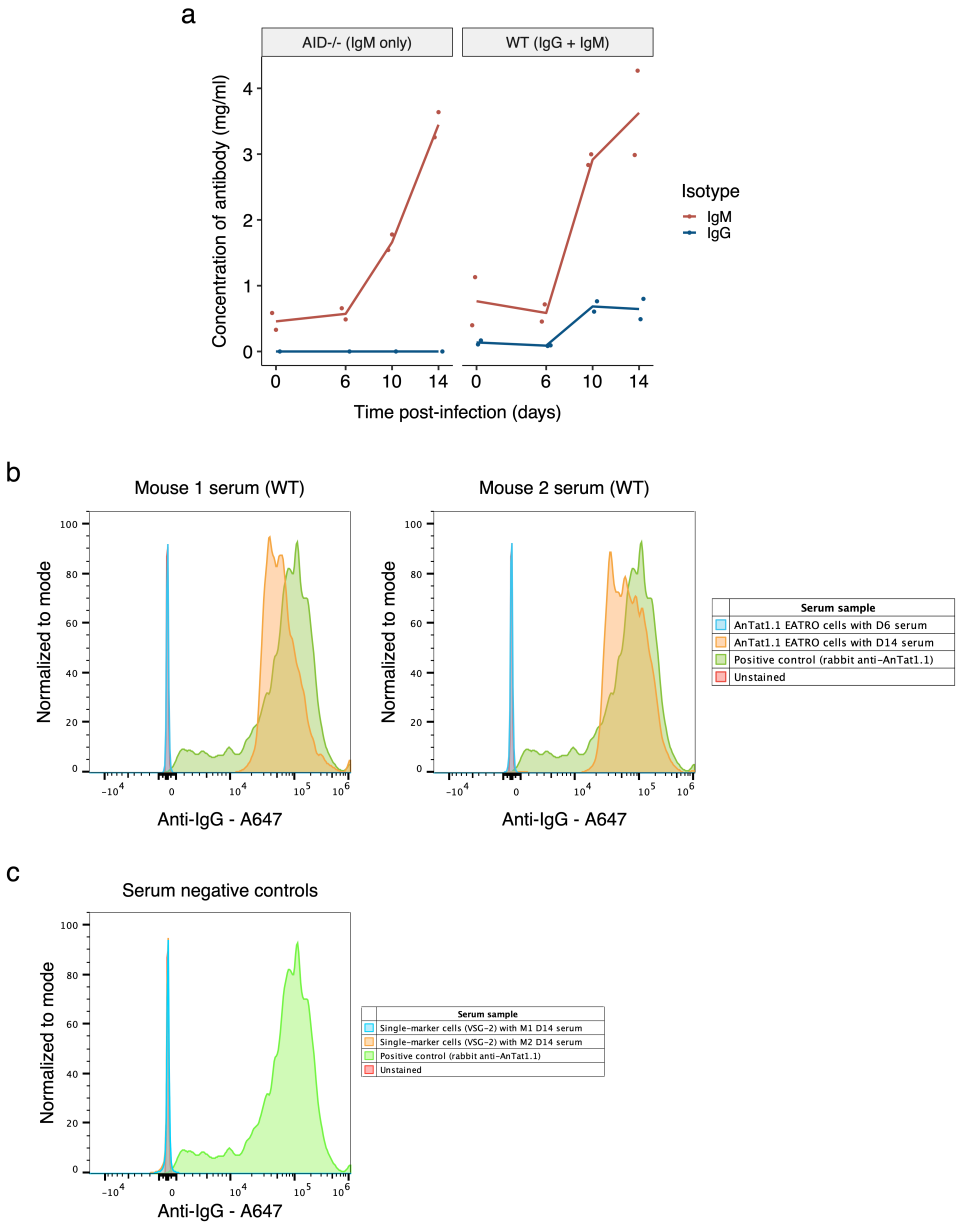

Extended Data Fig. 6. (a) Quantification of serum IgM and IgG concentrations in infected AID$^{-/-}$ and wildtype (WT) mice by ELISA (n = 2). (**b**) AnTat1.1 EATRO cells (expressing VSG AnTat1.1) stained with serum, followed by an anti-IgG secondary antibody that cross-reacts with IgM and other isotypes, from day 6 and day 14 of two mice infected with AnTat1.1 Triple-marker cells. A polyclonal rabbit anti-AnTat1.1 antibody on cells known to be expressing AnTat1.1 was used as a positive control. (**c**) Single-marker cells (expressing VSG-2) stained with day 14 serum from two mice infected with AnTat1.1 Triple-marker cells. These were used as negative controls to show that serum from infected mice specifically binds AnTat1.1 and no other VSGs.

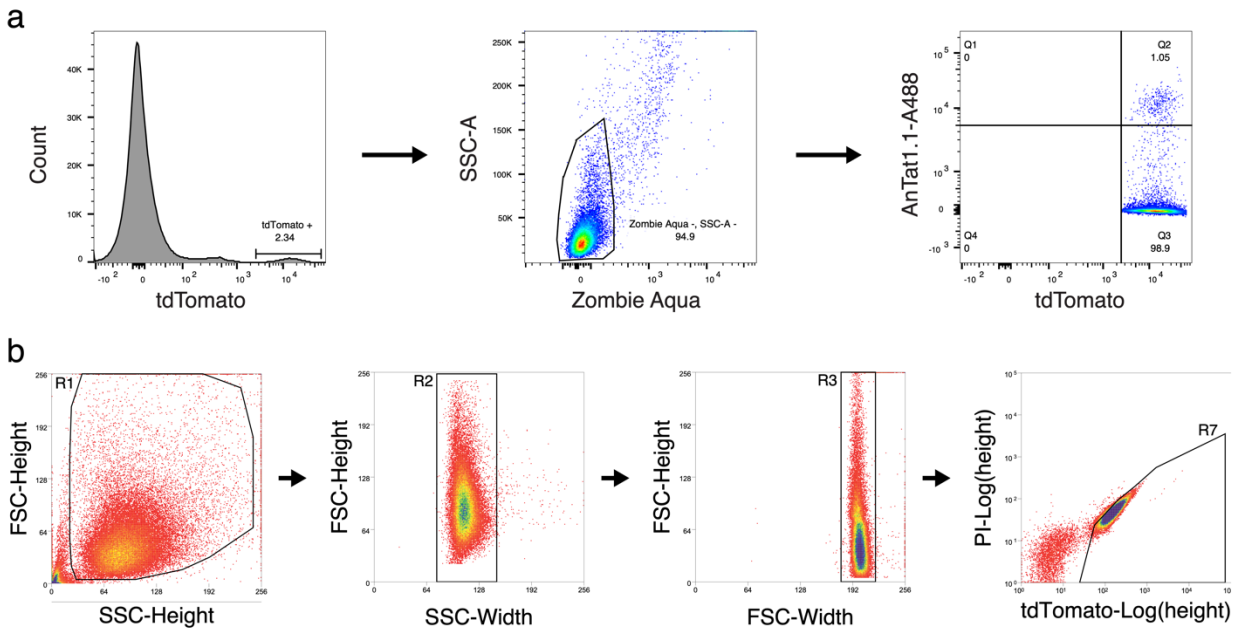

Extended Data Fig. 7. (**a**) Example gating strategy for flow cytometry experiments from Figure 3. Samples were first gated for tdTomato-positive cells, which represent *T. brucei* parasites expressing tdTomato in their cytoplasm. Then live cells were gated based on live/dead Zombie Aqua^{TM} staining. Finally, quadrants were placed around AnTat1.1-A488 positive and negative cells. (**b**) Gating strategy for single-cell sorting into 384-well plates for the SL-Smart-seq3xpress platform. This example is from the blood of mouse 2. Singlet parasites were selected and then tdTomato positive, PI (propidium iodide) negative *T. brucei* cells were sorted into single cells.

Summary table of the flow cytometry counts for tdTomato positive cells stained with an anti-AnTat1.1 antibody

Biological experiment	*Mouse*	*Tissue*	*Day*	*Count of AnTat1.1 + cells*	*Count of AnTat1.1 - cells*	*Total number of cells*	*Percent of cells AnTat1.1+*
1	1	blood	6	20394	486	20880	97.67%
1	1	gon. fat	6	411	32	443	92.78%
1	1	lung	6	817	49	866	94.34%
1	2	blood	6	42969	1458	44427	96.72%
1	2	blood	13	1	19922	19923	0.01%
1	2	gon. fat	13	0	250	250	0.00%
1	2	lung	13	573	4460	5033	11.38%
2	3	blood	6	19737	270	20007	98.65%
2	3	gon. fat	6	220	4	224	98.21%
2	3	lung	6	1464	55	1519	96.38%
2	4	blood	6	39373	592	39965	98.52%
2	4	gon. fat	6	379	10	389	97.43%
2	4	lung	6	676	30	706	95.75%
2	5	blood	6	49406	600	50006	98.80%
2	5	blood	13	1	19885	19886	0.005%
2	5	gon. fat	13	31	4982	5013	0.62%
2	5	lung	13	318	29889	30207	1.05%
2	6	blood	6	10317	31	10348	99.70%
2	6	blood	13	0	1001	1001	0.00%
2	6	gon. fat	13	3	781	784	0.38%
2	6	lung	13	265	29733	29998	0.88%
3	7	blood	6	65135	249	65384	99.62%
3	7	gon. fat	6	69	3	72	95.83%
3	7	lung	6	275	182	457	60.18%
3	8	blood	6	49239	632	49871	98.73%
3	8	gon. fat	6	71	0	71	100.00%
3	8	lung	6	770	137	907	84.90%
3	9	blood	6	49758	147	49905	99.71%
3	9	blood	13	3	5042	5045	0.06%
3	9	gon. fat	13	0	1537	1537	0.00%
3	9	lung	13	403	18944	19347	2.08%
3	10	blood	6	49286	642	49928	98.71%
3	10	blood	13	14	20204	20218	0.07%
3	10	gon. fat	13	33	7034	7067	0.47%
3	10	lung	13	187	38096	38283	0.49%

Extended Data Table 1. Flow cytometry counts of tdTomato-positive parasites from infections with triple-marker *T. brucei* parasites. Parasites were collected from the blood and dissociated tissues of 10 mice on either day 6 or 13 post-infection and stained with an anti-AnTat1.1 polyclonal antibody. Here we report the raw number of live tdTomato-positive parasites that were Antat1.1 positive and negative in each sample. These data were used to generate Fig. 3b.

Summary table of single cell sequencing results

		Number of single cells									
Mouse	*Tissue*	*Total cells sequenced*	*Cells passing QC cutoffs*	*Average successfully aligning UMI counts per cell*	*Cells with a de novo assemble d VSG ORF*	*1 VSG by alignment and 1 VSG by de novo assembly*	*>1 VSG by alignment and 1 VSG by de novo assembly*	*1 VSG by alignment and no VSG by de novo assembly*	*1 VSG by alignment and >1 VSG by de novo assembly*	*>1 VSG by alignment and >1 VSG by de novo assembly*	*>1 VSG by alignment and no VSG by de novo assembly*
Mouse 1	blood	370	238	5736	227	93	91	16	4	1	33
	gon. fat	370	227	4275	228	148	50	13	4	0	12
	heart	370	162	5375	201	125	36	1	0	0	0
	lung	370	123	2952	156	26	88	2	1	0	6
Mouse 2	blood	370	92	3572	148	50	35	5	1	0	1
	gon. fat	370	151	3997	133	106	16	22	1	1	5
	heart	370	156	4699	188	99	46	3	1	2	5
	lung	370	67	5097	96	42	23	0	0	0	2
Totals		2960	1216	4462	1377	689	385	62	12	4	64

Extended Data Table 2. Summary of single cell sequencing results. *T. brucei* single cells were sorted from blood and tissues on day 14 post-infection from 2 mice and sequenced using the SL-Smart-seq3xpress platform. For *de novo* assembly of VSGs, all cells were considered without filters, but for all other columns only cells that had at least 500 genes detected, 1000 gene UMI counts, 30 spike-in UMI counts, and 10 VSG UMI counts were considered. Additionally, only VSGs that had >1 UMI counts when aligning to the EATRO1125 genome were considered to be detected.

Supplementary information:

Supplementary Data 1: A summary of VSG expression in each cell by both genome alignment and *de novo* assembly, including categorization for Extended Data Figure 5e.

Supplementary Data 2: The EATRO1125 VSG read alignment in each cell that meets QC cutoffs (at least 500 genes detected, 1000 gene UMI counts, 30 spike-in UMI counts, and 10 VSG UMI counts) and has >1 VSG UMI count. Raw alignment count tables and VSG count tables that include unfiltered cells can also be found at https://github.com/mugnierlab/Beaver2022.

Supplementary Data 3: The results from *de novo* assembly of VSGs in each cell. The Trinity name for each ORF and the top VSG blast hit for each assembled VSG ORF is reported, including the proportion of VSG expression accounted for by that VSG. For each cell, a dominant VSG is identified if it represented over 80% of the VSG expressed in the cell and "NA" denotes that there is not a dominant VSG in that cell. VSG assembly was attempted in all cells without any previous QC filtering. Here, all VSG assemblies are reported without further filtering and the sequences can be found at https://github.com/mugnierlab/Beaver2022.